Enstatite chondrites EL3 as building blocks for the Earth: the debate 1 over the 146 Sm-142 Nd systematics

Maud Boyet, A. Bouvier, Paul Frossard, Tahar Hammouda, M. Garçon, Abdelmouhcine Gannoun

Enstatite chondrites EL3 as building blocks for the Earth: the debate over the ^{146}Sm-^{142}Nd systematics

M. Boyet[1], A. Bouvier[2], P. Frossard[1], T. Hammouda[1], M. Garçon[3], A. Gannoun[1]

[1] Laboratoire Magmas et Volcans, Université Clermont Auvergne, France

[2] Department of Earth Sciences, Centre for Planetary Science and Exploration, University of Western Ontario, London, Canada

[3] Department of Earth Sciences, ETH Zurich, Switzerland

Earth and Planetary Science Letters 488 (2018) 68–78

Keywords: ^{146}Sm-^{142}Nd systematics, enstatite chondrites, Earth's evolution, Earth's building blocks

Abstract

The ^{146}Sm-^{142}Nd extinct decay scheme (^{146}Sm half-life of 103 My) is a powerful tool to trace early Earth silicate differentiation. Differences in ^{142}Nd abundance measured between different chondrite meteorite groups and the modern Earth challenges the interpretation of the ^{142}Nd isotopic variations found in terrestrial samples because the origin of the Earth and the nature of its building blocks is still an ongoing debate. As bulk meteorites, the enstatite chondrites (EC) have isotope signatures that are the closest to the Earth value with an average small deficit of ~10 ppm in ^{142}Nd relative to modern terrestrial samples. Here we review all the Nd isotope data measured on EC so far, and present the first measurements on an observed meteorite fall Almahata

Sitta containing pristine fragments of an unmetamorphosed enstatite chondrite belonging to the EL3 subgroup. Once $^{142}Nd/^{144}Nd$ ratios are normalized to a common chondritic evolution, samples from the EC group (both EL and EH) have a deficit in ^{142}Nd but the dispersion is important ($\mu^{142}Nd$= -10 ± 12 (2SD) ppm). This scatter reflects their unique mineralogy associated to their formation in reduced conditions (low fO_2 or high C/O). Rare-earth elements are mainly carried by the sulfide phase oldhamite (CaS) that is more easily altered than silicates by weathering since most of the EC meteorites are desert finds. The EL6 have fractionated rare-earth element patterns with depletion in the most incompatible elements. Deviations in Nd mass independent stable isotope ratios in enstatite chondrites relative to terrestrial standard are not resolved with the level of analytical precision achieved by modern mass spectrometry techniques. Here we show that enstatite chondrites from the EL3 and EL6 subgroups may come from different parent bodies. Samples from the EL3 subgroup have Nd ($\mu^{142}Nd$= -0.8 ± 7.0, 2SD) and Ru isotope ratios undistinguishable from that of the Bulk Silicate Earth. EL3 samples have never been analyzed for Mo isotopes. Because these enstatite chondrites are relatively small in size and number, they are usually not available for destructive isotopic measurements. Average values based on the measurement of EL6 samples should not be considered as representative of the whole EL group because of melting and thermal metamorphism events affecting the Sm/Nd ratios and prolonged open-system history. The EL3 chondrites are the best candidates as the Earth's building blocks. These new results remove the need to change the composition of refractory incompatible elements early in Earth's history.

1. Introduction

Variations in mass independent stable isotope ratios, also called nucleosynthetic anomalies, of refractory elements have become extremely useful to trace the origin of the different planetary bodies and their relative contribution into the building process of terrestrial planets (e.g., Warren, 2011). Enstatite chondrites appear to be the closest in isotope composition to terrestrial samples and carbonaceous chondrites the furthest. Enstatite chondrites and the Earth are undistinguishable for many isotope systems, i.e. Cr, Ti, O, Ni (see Dauphas, 2017 for a recent review), meaning that with the current level of precision no resolvable difference is observed between both materials. A small difference in Si isotopes does exist and this has been used against the Enstatite Chondrite Earth model (Fitoussi and Bourdon, 2012) but Si isotopes may have been fractionated during nebular processes and their isotope ratios may not faithfully reflect the initial composition of the starting material (Savage and Moynier, 2013; Zambardi et al., 2013; Dauphas et al., 2015). The only resolvable differences between enstatite chondrites and the Earth were reported for Mo and Ru isotope compositions (Burkhardt et al., 2011; Fischer-Gödde and Kleine 2017). The enrichment in s-process Mo for the Earth relative to chondrites suggests that the composition of the Earth cannot be reconstructed by any known combination of meteorites because it is itself an end-member in the mixing trend (Burkhardt et al., 2011). The initial composition of the Earth has become an issue for the use and interpretation of the ^{146}Sm-^{142}Nd short-lived isotopic systematic in meteorites and Earth rocks. An early fractionation of the Sm/Nd ratio during the lifetime of ^{146}Sm ($T_{1/2}$=103 Ma) would modify the ^{142}Nd/^{144}Nd signatures by radiogenic production. In 2005, the first high-precision ^{142}Nd measurements in chondrites revealed a difference of about 20 ppm with the modern terrestrial samples (Boyet and Carlson, 2005). Because both Sm and Nd are

lithophile elements under terrestrial redox conditions (Bouhifd et al., 2015), a differentiation event of the silicate Earth in the first 30 Ma of Solar System history has been proposed to explain this offset. One type of model considers that the bulk Silicate Earth (BSE) preserves a relative chondritic abundance of refractory lithophile elements. The early-depleted mantle reservoir (high Sm/Nd) served as the source for magmatism since its formation whereas the enriched reservoir remains isolated from mantle convection and is still untapped (Boyet and Carlson, 2005). Other scenarios proposed that the complementary enriched reservoir (low Sm/Nd) has been lost to space by collisional erosion of planetesimals (Caro et al., 2008; O'Neill and Palme, 2008) leaving the Bulk Earth depleted in incompatible elements and with a higher Sm/Nd ratio relative to the well-constrained average composition of whole-rock chondrites from the carbonaceous (CC), ordinary (OC) and enstatite (EC) chondrite groups (Bouvier et al., 2008).

These models have been challenged by the discovery of variations in mass independent stable Sm and Nd isotope ratios in whole-rock chondrites and their components (Andreasen and Sharma, 2006; Carlson et al., 2007; Gannoun et al., 2011; Brennecka et al., 2013, Bouvier and Boyet, 2016; Burkhardt et al., 2016). The isotope ^{142}Nd is mainly produced by *s-process* but has a small contribution of *p-process*, estimated to be lower than a few percent (Arlandini et al., 1999; Bisterzo et al., 2011). The parent isotope, ^{146}Sm is a pure *p-process* nuclide so any variation in the *p* production would affect the abundance of its daughter isotope ^{142}Nd as well. Although we have undisputable evidences for different contribution of *s-process* isotopes in Solar System materials and measurable variations in the ^{142}Nd/^{144}Nd ratios, the origin of the terrestrial ^{142}Nd signature compared to the chondrite

meteorites is still unclear. The isotope signature of some ocean island basalts is difficult to interpret without an early event that would fractionate the Sm/Nd ratio of the bulk silicate Earth very early on in its history (Jackson et al., 2010). Here we re-evaluate the small isotopic variations measured in enstatite chondrites. Such meteorites were formed under reducing conditions and have a particular mineral assemblage. Importantly for interpreting their Sm-Nd systematics, half of the rare earth element (REE) budget is hosted in oldhamite (CaS), which is easily altered to Ca-sulphate by weathering (Crozaz and Lundberg, 1995; Gannoun et al., 2011).

We have compiled all the Nd isotope data published on EC so far. We also present the first measurements on an observed fall Almahata Sitta containing fragments of the EL3 subgroup, such as the fragment MS-177. The fireball of Almahata Sitta fall was captured on camera in northern Sudan on October 7th 2008. Its trajectory was back-tracked to a small asteroid called 2008 TC_3 (Bischoff et al., 2010). Additionally, REE concentration measurements are presented for samples belonging to the two subgroups of enstatite chondrites (EH and EL). Since the identification of ^{142}Nd variations attributed to nucleosynthetic anomalies requires a comparison at the same Sm/Nd evolution, we present in detail two methods of calculations used for normalization of all chondrites to a common Sm/Nd and the difficulties inherent to the enstatite chondrite sub-groups. The ^{142}Nd/^{144}Nd ratios are then compared to the corresponding mass independent stable Nd isotope ratios for each meteorite to establish their significance with respect to the distribution of nucleosynthetic anomalies amongst the chondrite groups. Finally, their potential contributions as Earth's building blocks are discussed.

2. Samples and Methods

2.1. Trace element contents in EC

Rare earth element concentrations have been measured for 12 EC from EH (4) and EL (8) sub-groups. The meteorite names and sample subgroups are reported in Table 1. Two techniques of dissolution have been used: 1) samples were digested in PFA Savillex® beakers using a mixture of concentrated HF-HNO_3 acids in 3:1 proportion at 120°C on hot plate during 48h; 2) samples were digested in individual Parr® pressure vessels in concentrated HF-HNO_3 (10:1) for 5 days at 155°C. In both cases, after drying down the samples, perchloric acid was added and evaporated on a hot plate to break down the fluorides. After successive dissolution/evaporation cycles in concentrated HNO_3, samples were taken back into solution in PFA Savillex® beakers or in Parr® pressure vessels in 6M HCl. All measurements were performed using the Agilent 7500 quadrupole ICP-MS at the Laboratoire Magmas et Volcans (LMV) in Clermont-Ferrand, with the exception of Almahata Sitta MS-177 and Hvittis that were measured at the University Western Ontario using a Thermo iCAP Qc quadrupole ICP-MS. Both ICP-MS are equipped with He collision cells. Samples were measured in HNO_3 0.5M- HF 0.05 M and HNO_3 0.3M- HF 0.01 M in the two laboratories, respectively. Counts per second were calibrated using rock standards BCR-2, BHVO-2 or BIR 1a. The rock standards and a synthetic standard solution (CMS) were routinely analyzed to validate the efficiency of the digestion procedures and the accuracy and precision of the acquired data. Blank and standard solutions were measured every 4 samples. Both the external reproducibility estimated from

repeated measurements of the standards and the accuracy checked from certified rock standard analyses are lower than 5%.

2.2. ^{146,147}Sm-^{142,143}Nd systematics and mass independent stable Nd isotopes

Here we report new results for MS-177 (Table 2). After the Parr bomb digestion of the samples at the University of Western Ontario, following the methods detailed in Bouvier and Boyet (2016), an aliquot of about ~80% was used for isotopic composition, ~10% fraction was spiked with an enriched ^{149}Sm-^{150}Nd mixed spike to determine precisely the Sm/Nd ratios by isotopic dilution, and another 10% aliquot was used to determine Q-ICPMS REE concentrations. The Sm and Nd of the spiked fractions were purified and separated using a two-stage chemistry procedure (cationic AG50W-X8 and Ln-spec resins). This procedure was also used for a BCR-2 USGS basalt standard (aliquot of 1.1 mg) to ensure accuracy and reproducibility of our spiked and unspiked measurements. Both spiked Sm and Nd isotopic fractions were analyzed using a MC-ICPMS Neptune Plus at LMV.

The separation procedure for the Nd isotopic composition required 3 steps as described in Garçon et al. (2018). The Ce was separated from other trivalent REE using the oxidation of Ce to Ce^{4+} on Ln-Spec resin (Tazoe et al., 2007; Li et al., 2015). Then the separation between Nd and Sm was achieved on Ln-Spec resin using 0.20N to 0.25N HCl. Total procedural blanks are genrally lower than a few tens of pg for Nd. The Nd isotopic compositions were measured as Nd^{+} using the LMV Triton Plus™ Multicollector Thermal Ionization Mass Spectrometer. For MS-177, Nd

isotope ratios were obtained in static mode following the method described in Gannoun et al. (2011a). Static measurements were preferred because the amount of Nd was small (~300 ng for MS-177) and dynamic routines require large sample size (e.g. 750 ng for the 4-line acquisition scheme developed by Garçon et al., 2018). In addition, we used a mass spectrometer equipped with new faraday collectors (6 month-old). No sign of deterioration of the faraday collectors was identified during the measurements. Ce and Sm contributions, monitored at masses 140 and 147 respectively, were lower than 3 ppm on masses 142 and 144 for both standard and sample measurements. Nd isotope ratios were corrected for mass fractionation to $^{146}Nd/^{144}Nd=0.7219$ using the exponential mass-fractionation law. The external reproducibility (2SD) calculated from 6 repeated measurements of the JNdi-1 standard is 5.6 ppm on $^{142}Nd/^{144}Nd$, 7.4 ppm on $^{143}Nd/^{144}Nd$, 4.4 ppm on $^{145}Nd/^{144}Nd$, 8.2 ppm on $^{148}Nd/^{144}Nd$, and 10.9 ppm on $^{150}Nd/^{144}Nd$ (Table 2).

3. Results

The new REE data are reported in Table 1 and compared to published values from Gannoun et al. (2011b) and Barrat et al. (2014) in Figure 1. Data from Kalleymen and Wasson (1986) is not shown in Figure 1 because they reported the concentrations of only 5 REEs (La, Sm, Eu, Yb, and Lu), which is insufficient to define proper REE patterns. All EH samples have flat REE patterns with concentrations very similar to those reported in CI, except Kota Kota (EH3) that is enriched in LREE (Figure 1A). This split is the most visibly weathered in color and texture of our collection, and the meteorite was described as a strongly weathered EC by Leitch and Smith (1982). The measured sub-chondritic $^{143}Nd/^{144}Nd$ ratio of Kota

Kota suggests that this sample has a complex history with several episodes of fractionation of the Sm/Nd ratio (Gannoun et al., 2011b). Two EH samples display unusual REE patterns: Galim (b) and LAP 0225 (Figure 1A, data from Barrat et al. 2014). They are classified as impact melt (IM) and their REE patterns are in agreement with the petrological description of the samples (Michel-Lévy and Bourot-Denise, 1988; Russel et al., 2004). EL samples present more variable REE distributions. Most of EL3 samples display flat REE patterns with concentrations ranging between 0.6 to 2 times the CI values. MAC 88180 is more enriched in REE (x2 CI) and has a negative Eu anomaly ($Eu/Eu^*=Eu_{CI}/(Sm_{CI}^{1/2} x\ Gd_{CI}^{1/2})$ of 0.7 (Figure 1C). Similar REE patterns have been obtained following the two dissolution techniques. Almahata Sitta MS-177, which is the most depleted EL3 sample, has a positive Eu anomaly of 1.5. The REE pattern for MS-177 is more similar to Adrar Bous (EL5) with lower REE contents and large positive Eu anomalies ($Eu/Eu^*=1.3$). EET 92063 has a REE pattern with similar characteristics but REE contents are even lower and the Eu positive anomaly is higher (Figure 1D). This sample is described as highly weathered and classified in an anomalous EL6 group by Barrat et al. (2014). By contrast, all other EL6 samples display negative Eu anomalies and are called "normal EL6" by the same authors. EL6 samples are all depleted in LREE relative to HREE ($(La/Lu)_N$) up to 0.62. Chemical heterogeneities are observed within the same sample. For example Hvittis has been measured 4 times and Eu/Eu* varies from 0.8 to 1.0 depending on the split analyzed. Petrological observations show that all these samples are strongly heterogeneous at millimeter to centimeter scale. Rare earth element distribution in the different EC subgroups is presented in Figure 2. This time, the database for REE in enstatite chondrites from Kallemeyn and Wasson (1986) is included. All subgroups have similar Yb concentrations but different $(La/Sm)_N$ ratios.

225 Strong depletions in incompatible elements, hence low La/Sm ratios, are measured in
226 EL6 samples and the two samples characterized by an unusual mineralogical
227 assemblage (Galim (b) and LAP 0225). Then EL6 samples are clearly different from
228 other EL samples. We note that the La/Sm ratios in EH are more variable and in
229 average higher than those measured in EL3-5 samples.

230 Measured Nd isotope ratios for MS-177 are expressed in ppm deviation
231 relative to the reference JNdi-1 standard (μ-value) in Table 2 and all details on
232 measurements (isotope ratios, intensity, interferences, etc) are available in
233 Supplementary information (Table S2). This sample presents a small deficit of -11
234 ppm in $^{142}Nd/^{144}Nd$ whereas all stable isotope ratios are identical within errors to the
235 JNdi-1 standard values. The $^{147}Sm/^{144}Nd$ ratios calculated using the isotope dilution
236 method are $^{147}Sm/^{144}Nd = 0.1381$ for the BCR-2 standard and 0.1897 for MS-177.
237 Our repeated spiked Sm-Nd measurements of BCR-2 standard at LMV give an
238 average of $^{147}Sm/^{144}Nd = 0.1381 \pm 0.0003$ (2SD, n=4), thus a precision of 0.2%. This
239 value is within literature values which range from $^{147}Sm/^{144}Nd = 0.1357$ to 0.1396 and
240 identical within errors with the most recent determination by ID TIMS at 0.1379
241 ±0.0002 (2SD; Li et al., 2012 and references therein). The initial $^{143}Nd/^{144}Nd$ ratio for
242 MS-177 calculated at 4.568 Ga is $\varepsilon^{143}Nd = +0.06 \pm 0.25$ when normalized to the initial
243 for the Solar System composition using the chondrite average (CHUR) $^{147}Sm/^{144}Nd$
244 and $^{143}Nd/^{144}Nd$ ratio values (Bouvier et al., 2008).
245
246
247 **4. Discussion**
248 **4.1. ^{146,147}Sm-^{142,143}Nd systematics in enstatite chondrites**
249

The purpose of this paper is to take a more rigorous look at enstatite chondrites and their genetic relationship to the Earth. To compare the compositions of enstatite chondrites to other chondrite groups, we compiled all Nd data published on chondrites from this group so far, as well as new data. This compilation is provided in supplementary materials. Available data comes from 7 different publications: Boyet and Carlson (2005); Rankenburg et al. (2006); Carlson et al. (2007); Gannoun et al. (2011); Bouvier and Boyet (2016); Burkhardt et al. (2016); and Fukai and Yokohama (2017). For the studies using La Jolla Nd standard for the calculation of deviation in ppm relative to the terrestrial value (μNd), the data were recalculated relative to the JNdi-1 terrestrial standard. The two synthetic standards La Jolla and AMES record significant mass-dependent variability and then cannot be used as a reference either for the BSE or the modern mantle (O'Neil et al., 2008; Gautam et al., 2017; Saji et al., 2016). All the measurements have been obtained on large-size samples (1-2 g). The Nd isotope compositions obtained for the Allende CV3 chondrite using different methods of digestion (table-top acid-digested, Parr bomb acid-digested and alkali-fused acid-digested samples) are similar (Boyet and Carlson, 2005; Carlson et al., 2007). The complete digestion of refractory components may be an issue for some elements but not for Nd. Presolar SiC grains are a primary carrier of large Ba isotope anomalies and the destruction of these grains during the digestion is required (Bermingham et al., 2016). When measuring the Nd isotope composition of extra-terrestrial materials, an additional consideration is to take into account the potential neutron capture effects due to the interaction of materials with galactic cosmic rays. However previous studies have measured very small deviations in the ^{149}Sm abundance of chondrites which is one of the Sm isotopes having the largest thermal neutron capture cross section. This suggests that chondrites have not been

significantly affected by neutron fluence effects and that the correction on $^{142}Nd/^{144}Nd$ ratios is negligible or within the measurement precision (e.g. Boyet and Carlson, 2005; Bouvier and Boyet, 2016). McCoy-West et al. (2017) have determined the mass-dependent stable Nd isotope composition using a double spike technique. Chondrites and terrestrial samples have identical isotopic compositions with $\delta^{146}Nd/^{144}Nd = -0.025 \pm 0.025$‰ (2SD; n=39) and $\delta^{146}Nd/^{144}Nd = -0.022 \pm 0.034$‰ (2SD; n=30) respectively. These results imply that no bias is produced by the correction of instrumental mass fractionation effects when processing the raw data.

The first high-precision ^{142}Nd measurements on chondrites have shown that differences in $^{142}Nd/^{144}Nd$ ratios existed among chondrite groups and that these variations were not correlated with changes of Sm/Nd ratios (Boyet and Carlson 2005). The new compilation combining all data measured on chondrites since 2005 leads to the same conclusion. The different groups of chondrites have different measured $^{142}Nd/^{144}Nd$ values (Figure 3A). We note that results obtained from different chondrite fragments which were processed in different labs using different analytical techniques are in good agreement. On average carbonaceous chondrites (CC) have a $\mu^{142}Nd$ of -31 ± 20 (2SD) ppm, ordinary chondrites (OC) of -16 ± 9 (2SD) ppm and EC of -12 ± 21 (2SD) ppm. Although standard deviations overlap, two sample t-tests strongly suggest that the three populations of chondrites are distinct from each other with p-values lower than 0.05 (p-value CC-OC = 1.5×10^{-8}; p-value CC-EC = 8.9×10^{-10}; p-value OC-EC = 0.004). Five samples have $^{147}Sm/^{144}Nd$ ratios far from the CHUR value of 0.1960 (dashed line in Figure 4A and 4B; Bouvier et al., 2008): NWA 2090 (CO3) and Tagish Lake (C2-ungrouped, not represented in the figure: $^{147}Sm/^{144}Nd$=0.148) for CC, Adrian (H4) for OC (not represented in the figure:

300 $^{147}Sm/^{144}Nd$=0.137), and Kota Kota and Blithfield for EC. Moreover one EC sample
301 displays an extreme $\mu^{142}Nd$ value and this measurement has a large error bar (Abee: -
302 44 ± 17 (2SE) ppm (Boyet and Carlson 2005). When all these samples are excluded
303 from the averaging calculation, CC have a $\mu^{142}Nd$ of -33 ± 16 (2SD) ppm, OC of -16
304 ± 9 (2SD) ppm and EC of -11 ± 12 (2SD) ppm. All these groups have similar
305 measured Sm/Nd ratios even if a larger range is observed for EC (Figure 4A, B).
306 When the same samples are selected, the mean $^{147}Sm/^{144}Nd$ ratios of each group is
307 0.1959 ± 0.0046 (2SD) for CC, 0.1946 ± 0.0033 (2SD) for OC and 0.1950 ± 0.0084
308 (2SD) for EC. The median values are equal to 0.1953, 0.1951 and 0.1952 for these 3
309 groups, respectively. CC and OC have normal distributions whereas EC present a
310 larger scatter. These values are slightly lower than the CHUR value of 0.1960 ±
311 0.0004 (2SD) defined from the average of unequilibrated chondrites (Bouvier et al.,
312 2008) but are similar within uncertainties. Two sample t-tests further confirm that the
313 mean $^{147}Sm/^{144}Nd$ ratios of the three populations are undistinguishable from each
314 other since p-values are much higher than 0.05 (p-value CC-OC = 0.9; p-value CC-
315 EC = 0.3; p-value OC-EC = 0.3).
316
317 The measured abundance of ^{142}Nd comes from two distinct contributions: its
318 initial abundance and the quantity produced with time by the decay of ^{146}Sm. Since
319 ^{146}Sm was alive only during the first 500 Ma of Solar System history, we can write
320 the following equations:
321 $$^{142}Nd_{meas} = {}^{142}Nd_{T0} + {}^{146}Sm_{T0} \quad (1)$$
322 $$(^{142}Nd/^{144}Nd)_{meas} = (^{142}Nd/^{144}Nd)_{T0} + (^{146}Sm/^{144}Nd)_{T0} \quad (2)$$

where $_{meas}$ denotes the abundance or isotopic composition measured today in chondrites and $_{T0}$ the initial abundance or isotopic composition at the time of formation.

These equations show that any fractionation of the Sm/Nd ratio during the ^{146}Sm lifetime will significantly affect the measured ^{142}Nd/^{144}Nd ratios. In order to compare initial ^{142}Nd/^{144}Nd ratios between chondrites, the data are thus corrected from the ^{142}Nd radiogenic production since the formation of the Solar System and normalized to a common chondritic evolution following the CHUR parameters defined by Bouvier et al. (2008). Two different methods of calculation can be used assuming a modification of the Sm/Nd ratio either early in the Solar system history or once the ^{146}Sm-^{142}Nd systematics is extinct.

Method A. ^{142}Nd/^{144}Nd corrected using measured ^{147}Sm/^{144}Nd ratios

This correction is illustrated in Figure 5A. The ^{142}Nd/^{144}Nd ratio of the sample is calculated back in time to the age of the Solar System formation, *i.e.* 4.568 Ga (Bouvier and Wadhwa, 2010) using the *measured* ^{147}Sm/^{144}Nd ratio. From this initial ^{142}Nd/^{144}Nd ratio, a modern value is recalculated using the CHUR ^{147}Sm/^{144}Nd ratio of 0.1960 (Bouvier et al., 2008). Such a correction assumes that the modification of the Sm/Nd ratio occurred at the beginning of Solar System history i.e. when the chondrites form.

Method B. ^{142}Nd/^{144}Nd corrected using measured ^{143}Nd/^{144}Nd ratios

This correction, illustrated in Figure 5B, does not consider the *measured* ^{147}Sm/^{144}Nd ratio but instead the *integrated* ^{147}Sm/^{144}Nd ratio calculated from the ^{147}Sm-^{143}Nd long-lived radiogenic systematics. Since recent changes of Sm/Nd ratios, for example

348 due to weathering, are not recorded in the evolution of $^{143}Nd/^{144}Nd$ ratios, the
349 $^{147}Sm/^{144}Nd$ ratio is deduced from the measured $^{143}Nd/^{144}Nd$ ratios considering that all
350 samples evolved from the same initial $^{143}Nd/^{144}Nd$ value of 0.506686 which
351 corresponds to the composition of the CHUR at 4.568 Ga (Bouvier et al., 2008).
352 Then, the normalized-CHUR $^{142}Nd/^{144}Nd$ ratio is calculated following the steps
353 described in Method A using the $^{147}Sm/^{144}Nd$ ratio of the CHUR from 4.568 Ga to
354 present-day.
355
356 To evaluate the influence of the chosen method on the CHUR-normalized
357 $\mu^{142}Nd$ values, we re-corrected all published $^{142}Nd/^{144}Nd$ ratios with the two methods
358 and compared the results in Figure 3B and C. Note that the Sm/Nd ratios of OC and
359 CC from Fukai and Yokoyama (2017) were measured by quadrupole ICPMS and are
360 thus reported with a much lower precision (1-1.5%) than that typically obtained
361 (about 0.2%) by isotope dilution with MC-ICPMS measurements of the spiked Sm
362 and Nd isotopic compositions. Such a large uncertainty on Sm/Nd ratios propagates to
363 errors of about 10 ppm on the CHUR-normalized $\mu^{142}Nd$ values. Fukai and
364 Yokoyama (2017) did not need to determine the precise $^{147}Sm/^{144}Nd$ ratios of their
365 samples because they used the method B to calculate their normalized $\mu^{142}Nd$ values.
366 However, we encourage future studies to systematically measure both the Nd isotope
367 composition and the corresponding Sm/Nd ratio at high precision using the isotope
368 dilution method.
369
370 Weighted averages for CC, OC and EC are -32 ± 13 (2SD), -15 ± 9 (2SD), -8
371 ± 15 (2SD) for the method A and -32 ± 13 (2SD), -16 ± 9 (2SD), and -10 ± 12 (2SD)
372 for the method B. Mean values are identical within errors but when looking at the data

373 in further details, significant differences are identified within the EC group. This is
374 illustrated in Figure 4C where both methods of correction are compared. For CC and
375 OC, all $^{142}Nd/^{144}Nd$ ratios plot along the 1:1 line whereas the EC show a larger
376 scatter. This scatter indicates that changes in the Sm/Nd ratios of EC have occurred at
377 different times, probably early in the Solar System history and recently by
378 weathering. The larger dispersion of the Sm/Nd ratios observed in EC may be
379 explained by their unique mineralogy as they formed under extreme reducing
380 conditions. Larimer and Bartholomay (1979) suggested that EC formed within a
381 region in the solar nebula with a high C/O ratio (>1). Although rare earth elements are
382 mainly carried by silicate minerals in other chondrite groups, about half of the Sm and
383 Nd elemental budget of EC is hosted in oldhamite, which is a Ca-sulfide (CaS). In-
384 situ measurements indicate that CaS are very rich in REE relative to CI chondrites (10
385 to 100 times the CI values; Crozaz and Lundberg, 1995; Gannoun et al., 2011b). In
386 EH3, the CaS have fractionated REE patterns with an enrichment in LREE relative to
387 HREE ($(La/Yb)_N$= 1-15) and positive anomalies in Eu and Yb (Crozaz and Lundberg,
388 1995; Gannoun et al., 2011b). Although in-situ REE measurements of CaS were
389 conducted only in EH3 samples, the measurements carried out in other groups of EC
390 and in aubrites (reduced enstatite achondrites) show diverse REE patterns which may
391 be associated with the weathering of CaS (Floss et al., 1990; Floss and Crozaz, 1993;
392 Crozaz and Lundberg, 1995). Petrological observations have shown that CaS are not
393 uniformly distributed in enstatite chondrites from EH and EL subgroups. In EH, CaS
394 is mainly included in metal-sulfide nodules even if it can be present in the matrix or in
395 chondrules dominated by silicate phases (El Goresy et al., 1988; Gannoun et al.,
396 2011b; Piani et al., 2016). Our observations of EL3 samples suggest that CaS is
397 mostly found in chondrules where it is intimately intergrown with enstatite and

398 occasionally with diopside (El Goresy et al., 2017). Its occurrence in metal-dominated
399 nodules is less common. Although metal-sulfide nodules are more subject to
400 oxidation/weathering than silicate assemblages, CaS enclosed in metal should be
401 better preserved because metal has no fracture veins like silicates. No clear
402 relationship has been found between REE fractionation and the type of samples
403 (group, fall *vs.* found, etc). To minimize the amplitude of the correction on
404 $^{142}Nd/^{144}Nd$ ratios and reduce the errors caused by a potential Sm/Nd fractionation
405 during weathering, we selected a subset of EC samples (11 samples, 16
406 measurements) with measured $^{147}Sm/^{144}Nd$ ratios very close to the CHUR value i.e.
407 between 0.1926 and 0.1994 (±1.7%). Within this range, the correction reaches a
408 maximum of ± 5 ppm on the $^{142}Nd/^{144}Nd$ ratios, i.e. equivalent to the average external
409 reproducibility. Taking only this subset of EC samples yields an average $\mu^{142}Nd$ of -
410 10 ± 12 (2SD) for the two methods A and B, hence does not change the mean nor
411 improve the standard deviation obtained for the whole EC group.
412
413
414 **4.2. Stable Nd isotope signature of EC relative to other groups**
415
416 Neodymium has 7 isotopes from mass 142 to 150. Nucleosynthetic anomalies,
417 which are mass-independent variations, can be identified by measuring 3 stable
418 isotope ratios: $^{145}Nd/^{144}Nd$, $^{148}Nd/^{144}Nd$ and $^{150}Nd/^{144}Nd$. Both $^{142}Nd/^{144}Nd$ and
419 $^{143}Nd/^{144}Nd$ are modified by radiogenic productions from ^{146}Sm and ^{147}Sm
420 respectively, and $^{146}Nd/^{144}Nd$ is used for internal mass bias correction and
421 normalization to a common ratio value of 0.7219. Except ^{142}Nd which is mainly
422 produced by *s-process* and ^{150}Nd which is a pure *r-process* nuclide, all other isotopes

423 are formed by a combination of *s*- and *r-processes* in different stellar environments
424 (Arlandini et al., 1999; Bisterzo et al., 2011). A change in the -*s*/-*r* proportions thus
425 modifies the Nd isotope patterns. Excess in s-process produces excess in ^{142}Nd and
426 deficits in ^{143}Nd, ^{145}Nd, ^{148}Nd and ^{150}Nd with the deficits increasing from mass 143 to
427 mass 150. Measurements obtained on individual EC are presented in Figure 6. The
428 average values for both CC and OC groups are shown for comparison. For clarity,
429 errors bars (2SD) are not shown in the figure but are instead provided in the figure
430 caption. The large errors calculated for CC reflect the variability of s-process nuclides
431 among this group owing to the contribution of CAIs. In a μ^{150}Nd vs μ^{148}Nd binary
432 plot, bulk CC and separated CAIs plot on the mixing line calculated from isotope
433 production in stellar models (see Fig. 3 in Bouvier and Boyet, 2016). CAIs can be the
434 carrier of large s-process excess signature with deficits in μ^{148}Nd and μ^{150}Nd of
435 several tens of ppm (Brennecka et al., 2013; Marks et al., 2014; Bouvier and Boyet,
436 2016).
437
438 The compositions of EC are scattered in the 3 binary plots without any clear
439 correlation (Figure 6). Results of mixing of the s-model prediction with the terrestrial
440 composition are indicated by the dashed lines depending on the model used: 1) stellar
441 model by Arlandini et al. (1999) or 2) using the composition of SiC as representative
442 of a pure s-process component (Hopp and Ott, 1997). Deficits in ^{142}Nd measured in
443 enstatite chondrites from the EH group and the EL6 subgroup are small and equal to -
444 11 ppm in average. For such small deficit, the expected deviations in 145, 148 and
445 150-Nd are equal to +5, +11 and +17 ppm, respectively. These variations remain very
446 small in comparison to the measurement precision (external reproducibility) obtained
447 with the last generation of multi-collector thermal ionization mass spectrometers

448 (TIMS). In the recent study of Burkhardt et al. (2016), both $^{142}Nd/^{144}Nd$ and
449 $^{148}Nd/^{144}Nd$ ratios were measured using a dynamic procedure leading to better
450 external reproducibilities than static measurements. The relative deterioration of the
451 Faraday collectors and their change of efficiency through time are important sources
452 of imprecision and inaccuracy for the determination of isotope ratios using static
453 multicollection (Makishima and Nakamura, 1991; Thirlwall, 1991). However, even
454 with dynamic procedures on TIMS, the external reproducibilities for $^{148}Nd/^{144}Nd$
455 reach 11 and 15 ppm on repeated measurements of the BHVO-2 rock standard and
456 JNdi-1 standard, respectively. Better precisions have been recently reported by Saji et
457 al. (2016) using multi-collector inductively coupled plasma mass spectrometry and a
458 sample-standard bracketing technique. Five measurements of the carbonaceous
459 chondrite Allende (CV3) give an external reproducibility of 1 ppm on the $^{148}Nd/^{144}Nd$
460 ratio with intensity of 14 V at mass 142. Because enstatite chondrites are about 2
461 times more depleted in Nd than CV3 carbonaceous chondrites, this technique would
462 require large quantities of EC samples (i.e. 2 g). A new 4-mass-step acquisition
463 scheme developed by Garçon et al. (2018) by thermal ionization mass spectrometry is
464 very promising because this routine is able to return all Nd isotope ratios dynamically
465 and provide a robust evaluation of the data to assess the quality of the data (e.g.,
466 mixing effects on the filament, fractionation between acquisition steps).
467
468
469 **4.3. The isotope similarity between EL3 samples and the Earth**
470
471 Amongst all the classified meteorites, enstatite chondrites represent only 2%
472 of the chondrites with 189 and 160 samples for the EH and the EL subgroups,

473 respectively. They have been distinguished on the basis of their Fe/Si bulk ratios as
474 high-Fe (EH) or low-Fe (EL) (Sears et al., 1982; Kallemeyn and Wasson, 1986). The
475 two EC subgroups also differ in their sulfide mineralogy. In addition to troilite (FeS),
476 daubréelite ($FeCr_2S_4$) and oldhamite, which are common to both EH and EL
477 subgroups, niningerite (MgS) is the diagnostic sulfide of EH, whereas alabandite
478 (MnS) is specific to EL. Most of enstatite chondrites are found objects that may have
479 been affected by weathering during their long residence time at the Earth surface. Fall
480 objects are extremely rare with only 7 samples for EH (2 EH3: Parsa and Qingzhen; 3
481 EH4: Abee, Adhi Kot, Indarch; 2 EH5: St. Mark's and Saint-Sauveur; Itqiy and
482 Galim (b) are classified as EH but present highly fractionated trace element patterns),
483 whereas 8 fall samples for EL are all from the EL6 group, except small fragments
484 from the newly discovered Almahata Sitta meteorite. This meteorite was classified as
485 a polymict ureilite and contains EC fragments of a few grams amongst a variety of
486 lithologies. Fragment MS-177 was originally assigned an equilibration grade as EL3/4
487 with claimed impact-melt metal pockets (Bischoff et al., 2010). In contrast, El Goresy
488 et al. (2017) argued for an origin by condensation based on the study of textures and
489 sulfide mineral chemistries. REE patterns reported for EL6 samples are fractionated
490 (Figure 1). Rubin et al. (2009) claims this depletion observed in many EL6 and some
491 more primitive EL as a result of impact processes. EL6 samples would then represent
492 a residuum largely depleted in LREE and Ca. No evidence for claimed impact melting
493 was reported by El Goresy et al. (2017) in any EH or EL investigated. The good
494 agreement observed between $\mu^{142}Nd$ values corrected using Methods A and B for EL6
495 samples supports a fractionation event early in the history of the parent body. Ar-Ar
496 isochron ages suggest closure of the K-Ar system at 4.45-4.49 Ga for EL5 and EL6
497 chondrites (Hopp et al., 2014).

When the $^{142}Nd/^{144}Nd$ ratios are classified by metamorphic types (Figure 7), there is no difference for samples from the EH group. In contrast, two different populations are distinguished for the EL samples. EL6 samples have a larger deficit in ^{142}Nd with an average of -12.7 ± 6.0 (2SD) ppm when corrected with method B. EL3 samples have a $\mu^{142}Nd$ value similar to the terrestrial standard within the error bars: -0.8 ± 7.0 (2SD) ppm. The p-value from two sample t-test yields 0.001, meaning that the EL3 and EL6 populations likely do not share the same ^{142}Nd means when corrected with method B. Samples form EL3 and EL6 subgroups are also statistically different when considering the two-sided Student's *t*-values 95% confidence intervals : $\mu^{142}Nd$ EL3= -0.8 ± 4.4 ppm and $\mu^{142}Nd$ EL6= -12.7 ± 2.3 ppm (see Table S1). This difference suggests either that EL3 and EL6 samples come from different parent bodies or that the correction for the ^{142}Nd radiogenic production is not correct for EL6 samples. The correction assumes an evolution over 4.568 Ga while Ar-Ar isochron on EL6 samples (Hopp et al., 2014) suggests a fractionation event 70 Ma after the beginning of the solar system history. Considering a two-stage evolution (chondritic $^{147}Sm/^{144}Nd$ ratio of 0.196 from T_0 to T_1 with T_0-T_1 = 70 Ma, the EL6 average $^{147}Sm/^{144}Nd$ ratio of 0.2005 from T_1 to present time shifts the correction by -2 ppm only. This average value $\mu^{142}Nd$ for EL6 remains statistically different from the EL3 subgroup. Another compelling result for the difference amongst EC compositions comes from the measurement of Ru isotopes (Fischer-Gödde and Kleine, 2017). Although the average of all EH and EL chondrites has a small deficit in $\varepsilon^{100}Ru$ (-0.08 ± 0.04, 95% confidence interval of the mean), the sample suite includes only one EL3 PCA 91020. This EL3 gave $\varepsilon^{100}Ru$ = +0.02 which is outside the 95% confidence interval of the average of the combined EL and EH data and similar to the Earth's

523 composition. A difference between Earth and EC has been reported for Mo isotopes
524 but no EL3 samples have been analyzed in this dataset meaning that the reported
525 average Mo isotopic composition of EC is based on EL6 samples only (Burkhardt et
526 al., 2011; Dauphas et el., 2002; Dauphas 2017). The Zn isotopic compositions of the
527 two EL3 chondrites measured by Moynier et al. (2011) are also identical to the
528 terrestrial values, whereas the analyzed EL6 chondrites are all enriched in heavy
529 isotopes and highly depleted in Zn. The origin of the volatile element depletion
530 between EL3 and EL6 chondrites can be explained by volatilization, probably during
531 thermal metamorphism. All these measurements suggest that EL samples do not come
532 from a single parent body. Similar conclusions were reached from petrographic and
533 geochemical observations for EH3 samples. Both normal and reverse MgS–FeS
534 zoning profiles in niningerite grains adjacent to troilite reveal an origin on different
535 parental asteroids with different MnS-contents in the niningerites (Lin and El Goresy,
536 2002; Gannoun et al., 2011b). At least 8 different parent bodies have been recently
537 proposed for the entire EC group based on chemical variations measured in sulfide
538 and metal phases (Weyrauch et al., 2017). However all these samples share very close
539 isotope signatures suggesting they condensed within the same region of the solar
540 nebula. Although our conclusion supports a genetic relationship between EL3 samples
541 and the Earth, this statement is based on the analysis of cosmochemical materials
542 present in our meteorite collection that represent a vey small record of materials
543 present in the Solar System. Recent high-precision Mo and Ru isotope measurements
544 have highlighted a terrestrial signature in IAB iron meteorites indicating that their
545 parent bodies could be the building blocks of the Earth (Worsham et al., 2017).
546 Unfortunately the lithophile behavior of REE makes it impossible to study these
547 meteorites for ^{146}Sm-^{142}Nd systematics.

548

549

550 **5. Conclusion**

551

552 Among all groups of chondrites, EC have measured $^{142}Nd/^{144}Nd$ ratios the
553 closest to the modern terrestrial signature ($\mu^{142}Nd$= -11 ±12 (2SD) ppm). In order to
554 compare initial $^{142}Nd/^{144}Nd$ ratios, data must be corrected from the ^{142}Nd radiogenic
555 production since the formation of the Solar System. Two methods of corrections are
556 compared (*measured* $^{147}Sm/^{144}Nd$ vs. *integrated* $^{147}Sm/^{144}Nd$ ratios). The two methods
557 yield results that are identical within the errors bars. Enstatite chondrites show a
558 larger scatter of Sm/Nd ratios in comparison to other chondrite groups that can be
559 attributed to early fractionation processes (e.g. samples from the EL6 subgroup)
560 and/or recent changes caused by weathering. In these chondrites, REE are mainly
561 concentrated in the calcium-sulfide phase (oldhamite), which is very sensitive to
562 weathering. For this latter reason we conclude that corrections based on *integrated*
563 $^{147}Sm/^{144}Nd$ ratios are more accurate for enstatite chondrites. The average of these
564 corrected values $\mu^{142}Nd$ give -10 ±12 (2SD) ppm. We report no significant variation
565 in the 3 stable Nd isotope ratios ($^{145}Nd/^{144}Nd$, $^{148}Nd/^{144}Nd$ and $^{150}Nd/^{144}Nd$) in EC
566 relative to terrestrial Nd standard.

567

568 When the $^{142}Nd/^{144}Nd$ ratios are ordered by enstatite chondrite sub-groups,
569 there is no difference for samples from the EH sub-group. In contrast, two different
570 populations are distinguished for the EL sub-group. EL6 samples have a larger deficit
571 in ^{142}Nd with an average of -12.7± 6.0 (2SD) ppm. EL3 samples have a $\mu^{142}Nd$ value
572 similar to the terrestrial standard within the error bars: -0.8 ± 7.0 (2SD) ppm. These

two populations are statistically different (p-values and 95% confidence interval uncertainties). These results are in agreement with those obtained for other elements (e.g. Zn and Ru) and suggest that 1) EL3 and EL6 samples do not come from the same parent body, and 2) EL3 samples are isotopically similar to the Earth. Because these enstatite chondrites are relatively small in size and number, they are usually not available for destructive isotopic measurements. Average values based on both the geochemical and isotopic compositions of EL6 samples should not be considered as representative of the whole EL group. The enstatite chondrite model (Javoy, 1995; Javoy et al., 2010, Kaminski and Javoy, 2013) considers instead that the Earth is built from essentially pure EH material for explaining the Mg/Si ratio of the Earth's upper mantle. A better knowledge on the mineralogy of the lower mantle and the proportion of silicon in the Earth's core could help in resolving this discrepancy.

Acknowledgments

Many thanks to Ahmed El Goresy for giving us this precious EL3 sample MS-177. We thank Christa Göpel and Maria Schönbächler for they invitation to present this study in the 2017 Goldschmidt session entitled "Presolar Grains and Isotopic Heterogeneity in Planetary Materials" and motivated to write this overview on this subject 12 years after the first high-precision ^{142}Nd measurements on chondrites were published. This project has received funding from the European Union's Horizon 2020 research and innovation program under Grant Agreement N° 682778). AB thanks support from the NSERC Discovery Grant and Canada Research Chair programs, and the France-Canada Research Fund. This is Laboratory of Excellence ClerVolc contribution number 286.

598

599

600 **References**

601 Anders, E., & Grevesse, N. (1989). Abundances of the elements: Meteoritic and solar.
602 *Geochimica et Cosmochimica acta*, *53*(1), 197-214.

603 Andreasen, R., Sharma, M. (2006). Solar nebula heterogeneity in p-process samarium
604 and neodymium isotopes. *Science*, *314*(5800), 806-809.

605 Arlandini, C., Käppeler, F., Wisshak, K., Gallino, R., Lugaro, M., Busso, M., &
606 Straniero, O. (1999). Neutron capture in low-mass asymptotic giant branch stars:
607 cross sections and abundance signatures. *The Astrophysical Journal*, *525*(2), 886-
608 900.

609 Barrat, J. A., Zanda, B., Jambon, A., & Bollinger, C. (2014). The lithophile trace
610 elements in enstatite chondrites. *Geochimica et Cosmochimica Acta*, *128*, 71-94.

611 Bermingham, K. R., Mezger, K., Scherer, E. E., Horan, M. F., Carlson, R. W.,
612 Upadhyay, D., ... & Pack, A. (2016). Barium isotope abundances in meteorites and
613 their implications for early Solar System evolution. *Geochimica et cosmochimica*
614 *acta*, *175*, 282-298.

615 Bischoff, A., Horstmann, M., Pack, A., Laubenstein, M., & Haberer, S. (2010).
616 Asteroid 2008 TC3—Almahata Sitta: A spectacular breccia containing many
617 different ureilitic and chondritic lithologies. *Meteoritics & Planetary Science*,
618 *45*(10 - 11), 1638-1656.

619 Bisterzo, S., Gallino, R., Staniero, O., Cristallo, S., Käppeler, F., 2011. The s-process
620 in lowmetallicity stars -II. Interpretation of high-resolution spectroscopic ob-
621 servations with asymptotic giant branch models. Mon. Not. R. Astron. Soc.418,
622 284–319.

623 Bouhifd, M. A., Boyet, M., Cartier, C., Hammouda, T., Bolfan-Casanova, N.,
624 Devidal, J. L., Andrault, D. (2015). Superchondritic Sm/Nd ratio of the Earth:
625 Impact of Earth's core formation. *Earth and Planetary Science Letters*, *413*, 158-
626 166.
627 Bouvier, A., Vervoort, J. D., & Patchett, P. J. (2008). The Lu–Hf and Sm–Nd isotopic
628 composition of CHUR: constraints from unequilibrated chondrites and
629 implications for the bulk composition of terrestrial planets. *Earth and Planetary*
630 *Science Letters*, *273*(1), 48-57.
631 Bouvier, A., & Wadhwa, M. (2010). The age of the Solar System redefined by the
632 oldest Pb-Pb age of a meteoritic inclusion. *Nature Geoscience*, *3*(9), 637-641.
633 Bouvier, A., Boyet, M. (2016). Primitive Solar System materials and Earth share a
634 common initial ^{142}Nd abundance. *Nature*, 537, 399-402.
635 Boyet, M., Carlson, R.W. (2005) ^{142}Nd Evidence for Early (>4.53 Ga) Global
636 Differentiation of the Silicate Earth. *Science*, 309, 576-581.
637 Brennecka, G. A., Borg, L. E., & Wadhwa, M. (2013). Evidence for supernova
638 injection into the solar nebula and the decoupling of r-process nucleosynthesis.
639 *Proceedings of the National Academy of Sciences*, 110, 17241-17246.
640 Burkhardt, C., Kleine, T., Oberli, F., Pack, A., Bourdon, B., Wieler, R. (2011).
641 Molybdenum isotope anomalies in meteorites: constraints on solar nebula
642 evolution and origin of the Earth. *Earth and Planetary Science Letters*, 312, 390-
643 400.
644 Burkhardt, C., Borg, L. E., Brennecka, G. A., Shollenberger, Q. R., Dauphas, N.,
645 Kleine, T. (2016). A nucleosynthetic origin for the Earth's anomalous 142Nd
646 composition. *Nature*, 537, 394-398.

647 Carlson, R.W., Boyet, M., Horan, M. (2007) Chondrite barium, neodymium, and
648 samarium isotopic heterogeneity and Early Earth Differentiation, Science, 316,
649 1175-1178.
650 Caro, G., Bourdon, B., Halliday, A. N., & Quitté, G. (2008). Super-chondritic Sm/Nd
651 ratios in Mars, the Earth and the Moon. *Nature*, 452, 336-339.
652 Crozaz, G., & Lundberg, L. L. (1995). The origin of oldhamite in unequilibrated
653 enstatite chondrites. *Geochimica et Cosmochimica Acta*, *59*, 3817-3831.
654 Dauphas, N. (2017). The isotopic nature of the Earth's accreting material through
655 time. *Nature*, *541*, 521-524.
656 Dauphas, N., Marty, B., & Reisberg, L. (2002). Inference on terrestrial genesis from
657 molybdenum isotope systematics. *Geophysical Research Letters*, *29*(6). 8.1-8.3
658 Dauphas, N., Poitrasson, F., Burkhardt, C., Kobayashi, H., & Kurosawa, K. (2015).
659 Planetary and meteoritic Mg/Si and δ30Si variations inherited from solar nebula
660 chemistry. *Earth and Planetary Science Letters*, *427*, 236-248.
661 El Goresy, A., Yabuki, H., Ehlers, K., Woolum, D., & Pernicka, E. (1988). Qingzhen
662 and Yamato-691: A tentative alphabet for the EH chondrites. In *Proceedings of the*
663 *NIPR Symposium on Antarctic Meteorites* (Vol. 1, pp. 65-101).
664 El Goresy, A., Lin, Y., Miyahara M., Gannoun A., Boyet M., Ohtani, E., Gillet, P.,
665 Trieloff, M., Simionovici, A., Feng, L., Lemelle, L. (2017). Origin of EL3
666 chondrites: evidences for variable C/O ratios during their course of formation – A
667 state of the art scrutiny. Meteoritics & Planetary Science, 52, 781–806.
668 Fitoussi, C., Bourdon, B. (2012) Silicon isotope evidence against an enstatite
669 chondrite Earth. Science, 335, 1477-1480.
670 Fischer-Gödde, M., Kleine T. (2017) Ruthenium isotopic evidence for an inner Solar
671 System origin of the late veneer. Nature, 541, 525-527. doi:10.1038/nature21045.

672 Floss, C., & Crozaz, G. (1993). Heterogeneous REE patterns in oldhamite from
673 aubrites: Their nature and origin. *Geochimica et Cosmochimica Acta*, *57*, 4039-
674 4057.
675 Floss, C., Strait, M. M., & Crozaz, G. (1990). Rare earth elements and the
676 petrogenesis of aubrites. *Geochimica et Cosmochimica Acta*, *54*, 3553-3558.
677 Fukai, R., & Yokoyama, T. (2017). Neodymium isotope heterogeneity of ordinary
678 and carbonaceous chondrites and the origin of non-chondritic 142Nd compositions
679 in the Earth. *Earth and Planetary Science Letters*, *474*, 206-214.
680 Gannoun, A., Boyet, M., Rizo, H., El Goresy, A. (2011a). ^{146}Sm–^{142}Nd systematics
681 measured in enstatite chondrites reveals a heterogeneous distribution of ^{142}Nd in
682 the solar nebula. *Proceedings of the National Academy of Sciences*, 108, 7693-
683 7697.
684 Gannoun, A., Boyet, M., El Goresy, A., Devouard, B. (2011b). REE and actinide
685 microdistribution in Sahara 97072 and ALHA77295 EH3 chondrites. *Geochimica*
686 *et Cosmochimica Acta*, 75, 3269-3289.
687 Gautam, I., Ray, J. S., Bhutani, R., Balakrishnan, S., & Dash, J. K. (2017). Role of
688 fractionation correction in accurate determination of 142Nd/144Nd by TIMS: A
689 case study of 1.48 Ga alkaline rocks from Khariar, India. *Chemical Geology*, *466*,
690 479-490.
691 Garçon M., Boyet M., Carlson R.W., Horan M.F., Auclair D., Mock T.D. (2018)
692 Factors influencing the precision and accuracy of Nd isotope measurements by
693 thermal ionization mass spectrometry. *Chemical Geology*, *476*, 493-514.
694 Hopp, J., Trieloff, M., Ott, U., Korochantseva, E. V., & Buykin, A. I. (2014). 39Ar -
695 40Ar chronology of the enstatite chondrite parent bodies. *Meteoritics & Planetary*
696 *Science*, *49*, 358-372.

697 Hoppe, P., & Ott, U. (1997). Mainstream silicon carbide grains from meteorites. In
698 *AIP Conference Proceedings*, 402, No. 1, pp. 27-58.
699 Izawa, M. R. M., King, P. L., Flemming, R. L., Peterson, R. C., & McCausland, P. J.
700 A. (2010). Mineralogical and spectroscopic investigation of enstatite chondrites by
701 X - ray diffraction and infrared reflectance spectroscopy. *Journal of Geophysical*
702 *Research: Planets, 115(E7). E07008, doi:10.1029/2009JE003452*
703 Jackson, M. G., Carlson, R. W., Kurz, M. D., Kempton, P. D., Francis, D., &
704 Blusztajn, J. (2010). Evidence for the survival of the oldest terrestrial mantle
705 reservoir. *Nature*, *466*, 853-858.
706 Javoy, M. (1995). The integral enstatite chondrite model of the Earth. *Geophysical*
707 *Research Letters*, *22*(16), 2219-2222.
708 Javoy, M., Kaminski, E., Guyot, F., Andrault, D., Sanloup, C., Moreira, M., ... &
709 Jaupart, C. (2010). The chemical composition of the Earth: Enstatite chondrite
710 models. *Earth and Planetary Science Letters*, *293*(3), 259-268.
711 Kallemeyn, G. W., & Wasson, J. T. (1986). Compositions of enstatite (EH3, EH4, 5
712 and EL6) chondrites: Implications regarding their formation. *Geochimica et*
713 *Cosmochimica Acta*, *50*, 2153-2164.
714 Kaminski, E., & Javoy, M. (2013). A two-stage scenario for the formation of the
715 Earth's mantle and core. *Earth and Planetary Science Letters*, *365*, 97-107.
716 Larimer, J. W., & Bartholomay, M. (1979). The role of carbon and oxygen in cosmic
717 gases: Some applications to the chemistry and mineralogy of enstatite chondrites.
718 *Geochimica et Cosmochimica Acta*, *43*, 1455-1466.
719 Leitch, C. A., & Smith, J. V. (1982). Petrography, mineral chemistry and origin of
720 Type I enstatite chondrites. *Geochimica et Cosmochimica Acta*, *46*(11), 2083-
721 2097.

Li, C. F., Li, X. H., Li, Q. L., Guo, J. H., Li, X. H., Feng, L. J., & Chu, Z. Y. (2012). Simultaneous determination of $^{143}Nd/^{144}Nd$ and $^{147}Sm/^{144}Nd$ ratios and Sm–Nd contents from the same filament loaded with purified Sm–Nd aliquot from geological samples by isotope dilution thermal ionization mass spectrometry. *Analytical chemistry*, *84*(14), 6040-6047.

Li, C.-F., Wang, X.-C., Li, Y.-L., Chu, Z.-Y., Guo, J.-H., Li, X.-H., 2015. Ce–Nd separation by solid-phase micro-extraction and its application to high-precision 142Nd/144Nd measurements using TIMS in geological materials. J. Anal. At. Spectrom. 30, 895–902. http://dx.doi.org/10.1039/C4JA00328D.

Lin, Y, & El Goresy, A. (2002). A comparative study of opaque phases in Qingzhen (EH3) and MacAlpine Hills 88136 (EL3): Representatives of EH and EL parent bodies. *Meteoritics & Planetary Science*, *37*(4), 577-599.

Makishima, A., & Nakamura, E. (1991). Calibration of Faraday cup efficiency in a multicollector mass spectrometer. *Chemical Geology: Isotope Geoscience section*, *94*(2), 105-110.

Marks, N. E., Borg, L. E., Hutcheon, I. D., Jacobsen, B., & Clayton, R. N. (2014). Samarium–neodymium chronology and rubidium–strontium systematics of an Allende calcium–aluminum-rich inclusion with implications for 146 Sm half-life. *Earth and Planetary Science Letters*, *405*, 15-24.

McCoy-West, A. J., Millet, M. A., & Burton, K. W. (2017). The neodymium stable isotope composition of the silicate Earth and chondrites. *Earth and Planetary Science Letters*, *480*, 121-132.

Michel-Lévy, M. C., & Bourot-Denise, M. (1988). A new look at the Galim (a) and Galim (b) meteorites. *Mineral. Mag*, *52*, 519-525.

746 Moynier, F., Paniello, R. C., Gounelle, M., Albarède, F., Beck, P., Podosek, F., &
747 Zanda, B. (2011). Nature of volatile depletion and genetic relationships in enstatite
748 chondrites and aubrites inferred from Zn isotopes. *Geochimica et Cosmochimica*
749 *Acta*, *75*(1), 297-307.
750 O'Neil, J., Carlson, R. W., Francis, D., & Stevenson, R. K. (2008). Neodymium-142
751 evidence for Hadean mafic crust. *Science*, *321*(5897), 1828-1831.
752 O'Neill, H. S. C., & Palme, H. (2008). Collisional erosion and the non-chondritic
753 composition of the terrestrial planets. *Philosophical Transactions of the Royal*
754 *Society of London A: Mathematical, Physical and Engineering Sciences*,
755 *366*(1883), 4205-4238.
756 Piani, L., Marrocchi, Y., Libourel, G., & Tissandier, L. (2016). Magmatic sulfides in
757 the porphyritic chondrules of EH enstatite chondrites. *Geochimica et*
758 *Cosmochimica Acta*, *195*, 84-99.
759 Rankenburg, K., Brandon, A. D., & Neal, C. R. (2006). Neodymium isotope evidence
760 for a chondritic composition of the Moon. *Science*, *312*(5778), 1369-1372.
761 Rubin, A. E., Huber, H., & Wasson, J. T. (2009). Possible impact-induced refractory-
762 lithophile fractionations in EL chondrites. *Geochimica et Cosmochimica Acta*,
763 *73*(5), 1523-1537.
764 Russell, S. S., Folco, L., Grady, M. M., Zolensky, M. E., Jones, R., Righter, K., ... &
765 Grossman, J. N. (2004). The meteoritical bulletin, no. 88, 2004 July. *Meteoritics &*
766 *Planetary Science*, *39*(S8).
767 Saji, N. S., Wielandt, D., Paton, C., & Bizzarro, M. (2016). Ultra-high-precision Nd-
768 isotope measurements of geological materials by MC-ICPMS. *Journal of*
769 *analytical atomic spectrometry*, *31*(7), 1490-1504.

770 Savage, P. S., Moynier, F. (2013). Silicon isotopic variation in enstatite meteorites:
771 clues to their origin and Earth-forming material. *Earth and Planetary Science*
772 *Letters*, *361*, 487-496.
773 Sears, D. W., Kallemeyn, G. W., & Wasson, J. T. (1982). The compositional
774 classification of chondrites: II The enstatite chondrite groups. *Geochimica et*
775 *Cosmochimica Acta*, *46*(4), 597-608.
776 Tazoe, H., Obata, H., & Gamo, T. (2007). Determination of cerium isotope ratios in
777 geochemical samples using oxidative extraction technique with chelating resin.
778 *Journal of Analytical Atomic Spectrometry*, *22*(6), 616-622.
779 Thirlwall, M. F. (1991). Long-term reproducibility of multicollector Sr and Nd
780 isotope ratio analysis. *Chemical Geology: Isotope Geoscience section*, *94*(2), 85-
781 104.
782 Warren, P. H. (2011). Stable-isotopic anomalies and the accretionary assemblage of
783 the Earth and Mars: A subordinate role for carbonaceous chondrites. *Earth and*
784 *Planetary Science Letters*, *311*(1), 93-100.

Weyrauch, M., Horstmann, M., & Bischoff, A. (2017). Chemical variations of sulfides and metal in enstatite chondrites—Introduction of a new classification scheme. *Meteoritics & Planetary Science*, 1-22.

Worsham, E. A., Walker, R. J., & Bermingham, K. R. (2016). High-precision molybdenum isotope analysis by negative thermal ionization mass spectrometry. *International Journal of Mass Spectrometry*, *407*, 51-61.

785 Worsham, E. A., Bermingham, K. R., & Walker, R. J. (2017). Characterizing
786 cosmochemical materials with genetic affinities to the Earth: Genetic and
787 chronological diversity within the IAB iron meteorite complex. *Earth and*
788 *Planetary Science Letters*, *467*, 157-166.

Zambardi, T., Poitrasson, F., Corgne, A., Méheut, M., Quitté, G., & Anand, M. (2013). Silicon isotope variations in the inner solar system: Implications for planetary formation, differentiation and composition. *Geochimica et Cosmochimica Acta*, *121*, 67-83.

List of Figures

Figure 1. Rare earth element (REE) patterns measured in enstatite chondrites from both EH and EL subgroups normalized to CI chondrites (Anders and Grevesse, 1989). New data are represented in black and Grey fields/line are data from Barrat et al. (2014) A) EH3 and impact melts (IM). LAP 02225 is an impact melt (Antarctic meteorite newsletter, Izawa et al., 2010). Galim is an unusual LL/EH polymict breccia with two lithologies: Galim (a) is a heavily-shocked LL6 chondrite and Galim (b) an impact melt breccia. Kota Kota (EH3) displays a strong enrichment in LREE. B) EH4 and EH5. Abee (EH4) is enriched in REE compared to other samples from the EH4 and EH5 groups. C) EL3 and one meteorite from the EL5 subgroup (Adrar Bous). MAC 88180 (two dissolutions) has two patterns that are both strongly enriched. Almahata Sitta MS-177 has the lowest REE contents. D) EL6 meteorites. All EL6 samples present very similar REE patterns, except EET 92063 described as highly weathered and classified in an anomalous EL6 by Barrat et al. (2014).

Figure. 2. $(La/Sm)_N$ normalized to CI chondrites using the values of Anders and Grevesse, (1989) compared with Yb contents (in ppm) for EC samples. Data are from this study and literature data from Gannoun et al. (2011b), Barrat et al. (2014) and Kalleymen and Wasson (1986). IM: impact melt.

814

815 **Figure. 3**. Compilation of μ^{142}Nd values (in ppm) in carbonaceous, ordinary and
816 enstatite chondrites. For each individual data point, errors bars show internal errors
817 (i.e. in-run errors, 2SE) or 2SD when several replicates of the same sample were
818 measured. Vertical pale yellow bands represent the mean of each chondrite groups
819 ±2SD and vertical green bands represent 95% confidence intervals. A) Measured
820 μ^{142}Nd expressed in part per million (ppm) deviations relative to the measured
821 standard values. B) μ^{142}Nd normalized to the CHUR ^{147}Sm/^{144}Nd following the
822 correction method A. C) μ^{142}Nd normalized to the CHUR ^{147}Sm/^{144}Nd value
823 following the correction method B. See Figure 5 and text for further details. Literature
824 data are from: Boyet and Carlson (2005); Andreasen and Sharma (2006); Carlson et
825 al. (2007); Gannoun et al. (2011a); Bouvier and Boyet (2016); Burkhardt et al.
826 (2016); Fukai and Yokohama (2017); and this study for Almahata Sitta MS-177. All
827 values are shown but six samples were removed from calculated weighted averages
828 reported in the figure caption for their respective groups because they have either
829 highly fractionated Sm/Nd ratios (Tagish Lake, NWA 2090, Adrian, Kota Kota and
830 Blithfiled) or correspond to a single run with a large internal uncertainty meaning that
831 the measurement is not reliable (Abee). Weighted mean values for CC are: -33 (± 16,
832 ± 4 for 2SD and 95% confidence interval, respectively); -32 (± 13; ± 3), -32 (± 13; ±
833 3) in graphs A, B and C. Weighted mean values for OC are: -16 (± 9, ± 2); -15 (± 9;
834 ± 2), -16 (± 9; ± 2) in graphs A, B and C. Weighted mean values for EC are: -11 (±
835 12, ± 2); -9 (± 15; ± 3), -10 (± 12; ± 2) in graphs A, B and C. Number of
836 measurements is 20 (10 samples) for CC, 28 (24 samples) for OC and 29 (17 samples)
837 for EC. Individual values and calculations (averages, errors) are reported in Table S1.
838

839 **Figure 4.** A. Compilation of measured $\mu^{142}Nd$ vs. $^{147}Sm/^{144}Nd$ for the different
840 chondrite samples. The line corresponds to a slope for a 4.568 Ga isochron. Here the
841 line is forced through the mean value of the ordinary chondrites group. B. Histogram
842 showing the distribution of measured $^{147}Sm/^{144}Nd$ ratios in the different groups of
843 chondrites. C. Comparison of the $\mu^{142}Nd$ normalized to the chondritic evolution
844 following the two calculation methods (A vs B) explained in the main text and shown
845 schematically in Figure 5. D. Same diagram as C for EC samples only.
846
847
848 **Figure 5**. Schematic illustration of the correction method for the normalization of
849 $^{142}Nd/^{144}Nd$ ratios to a common chondritic evolution. A. Method A using the
850 measured $^{147}Sm/^{144}Nd$ ratio of the sample. B. Method B using the calculated Sm/Nd
851 ratio from the long-lived ^{147}Sm-^{143}Nd systematics. T_0 is the age of the Solar System
852 formation, i.e. 4.568 Ga (Bouvier and Wadhwa, 2010). More details can be found in
853 the text. The CHUR parameters are those defined by Bouvier et al. (2008).
854
855 **Figure 6.** A. Mass independent stable Nd isotope composition of enstatite chondrites
856 $\mu^{142}Nd$ corr. B vs $\mu^{148}Nd$; B. $\mu^{145}Nd$ vs $\mu^{148}Nd$; C. $\mu^{145}Nd$ vs $\mu^{150}Nd$. Average values
857 ± 2SD (all in ppm) for CC are -32 ± 13 ($\mu^{142}Nd$), 4 ± 19 ($\mu^{145}Nd$), 16 ± 27 ($\mu^{148}Nd$)
858 and 17 ± 68 ($\mu^{150}Nd$). For OC: -15 ± 9 ($\mu^{142}Nd$), 3 ± 15 ($\mu^{145}Nd$), 7 ± 15 ($\mu^{148}Nd$) and
859 14 ± 54 ($\mu^{150}Nd$). CC data include 20 measurements on 10 samples. For OC, a total of
860 29 measurements carried out on 25 different samples are considered. For comparison,
861 the average values obtained from OC data published in Burkhardt et al. (2016) are -
862 18±6 ($\mu^{142}Nd$), 6±9 ($\mu^{145}Nd$), 7±8 ($\mu^{148}Nd$) and 17±13 ($\mu^{150}Nd$) (all in ppm). Dashed
863 lines (long and short respectively) represent mixing of the s-model prediction with the

terrestrial composition following: 1) stellar model by Arlandini et al. (1999), and 2) using the composition of SiC as representative of a pure s-process component (Hopp and Ott, 1997). External reprodubilities are not provided because this compilation includes data obtained by different authors and using different techniques.

Figure 7. Corrected μ^{142}Nd (normalized to the chondritic evolution using method B) in enstatite chondrites. Samples are ordered by groups. Fall meteorite samples are shown in bold.

List of Tables

Table 1. Rare Earth element contents of enstatite chondrites measured by ICP-MS. Two methods of acid digestion were used: (A) in PFA Savillex® beakers on hot plate at atmospheric pressure, (b) into individual pressurized Parr® bombs.

Table 2. Measured Nd isotope composition of the JNdi-1 standard and MS-177 (EL3). Errors correspond to the external reproducibility for the JNdi-1 standard runs (2SD) and internal error for MS-177. $^{147}Sm/^{144}Nd$ ratio has been measured by isotope dilution. The initial ε^{143}Nd is calculated at 4.568 Ga using the CHUR parameters defined by Bouvier et al. (2008). The average values measured for the terrestrial standard (n=7) are 1.141850 ± 6 for $^{142}Nd/^{144}Nd$, 0.512111 ± 4 for $^{143}Nd/^{144}Nd$, 0.348403 ± 2 for $^{145}Nd/^{144}Nd$, 0.241578 ± 2 $^{148}Nd/^{144}Nd$, and 0.236446 ± 3 for $^{150}Nd/^{144}Nd$ (see details in Table S2).

Table 1.
Rare Earth Elements measured in enstatite chondrites by ICP-MS
* Results already published in Gannoun et al. (2011b)
# Dissolution A) in PFA Savillex® beakers on hot plate at atmospheric pressure, B) into individual pressurized Parr® bombs.
[a] mass of the aliquot uptaken for measuring REE that corresponds to 5% of the total dissolution

sample	ALHA	Sahara	Sahara	Sahara	Kota Kota	Abee	Indarch	St Mark's	MAC	MAC	MAC	MAC	MS-177	Adrar	Eagle	Hvittis	Hvittis	Hvittis	Hvittis	Khairpur
name	77295*	97072*	97096*	97158*					02837	02839	88180	88180		Bous						
type	EH3	EH3	EH3	EH3	EH3	EH4	EH4	EH5	EL3	EL3	EL3	EL3	EL3	EL5	EL6	EL6	EL6	EL6	EL6	EL6
Fall						X	X	X					X		X	X	X	X	X	X
weight (g)	0.05	0.05	0.05	0.05	0.05	0.16	0.05	0.05	0.05	0.05	0.12	0.13	0.08[a]	0.11	0.05	0.12	0.10	0.10	0.05[a]	0.05
dissolution #	A	A	A	A	A	B	A	A	A	A	A	B	B	B	A	A	A	A	B	A
La	0.247	0.233	0.237	0.231	0.506	0.274	0.222	0.215	0.247	0.265	0.449	0.432	0.156	0.192	0.189	0.141	0.136	0.181	0.250	0.175
Ce	0.556	0.545	0.590	0.542	1.235	0.721	0.555	0.542	0.616	0.663	1.174	1.113	0.379	0.488	0.509	0.392	0.350	0.487	0.677	0.457
Pr	0.087	0.086	0.093	0.087	0.162	0.110	0.089	0.086	0.097	0.103	0.176	0.169	0.056	0.075	0.084	0.062	0.063	0.077	0.107	0.074
Nd	0.423	0.438	0.455	0.435	0.749	0.557	0.433	0.416	0.480	0.530	0.895	0.847	0.290	0.381	0.442	0.326	0.326	0.401	0.571	0.374
Sm	0.144	0.123	0.146	0.132	0.207	0.183	0.144	0.134	0.158	0.168	0.307	0.278	0.096	0.121	0.136	0.112	0.111	0.137	0.193	0.124
Eu	0.053	0.049	0.054	0.049	0.071	0.059	0.053	0.052	0.058	0.062	0.080	0.076	0.054	0.060	0.047	0.045	0.044	0.048	0.058	0.050
Gd	0.205	0.188	0.209	0.191	0.269	0.256	0.204	0.196	0.226	0.243	0.390	0.374	0.133	0.177	0.212	0.160	0.165	0.196	0.264	0.179
Tb	0.035	0.034	0.037	0.033	0.044	0.045	0.035	0.035	0.038	0.041	0.073	0.069	0.025	0.030	0.036	0.029	0.028	0.035	0.049	0.031
Dy	0.244	0.250	0.257	0.232	0.301	0.317	0.245	0.236	0.268	0.295	0.474	0.449	0.174	0.208	0.254	0.201	0.207	0.243	0.337	0.221
Ho	0.054	0.053	0.057	0.051	0.063	0.069	0.054	0.051	0.059	0.064	0.103	0.097	0.039	0.047	0.058	0.044	0.045	0.052	0.073	0.050
Er	0.161	0.160	0.172	0.156	0.189	0.201	0.160	0.154	0.174	0.194	0.306	0.294	0.120	0.142	0.174	0.139	0.142	0.160	0.218	0.147
Tm	0.023	0.022	0.027	0.023	0.028	0.030	0.025	0.023	0.026	0.029	0.047	0.045	0.018	0.021	0.027	0.022	0.023	0.025	0.032	0.023
Yb	0.155	0.150	0.174	0.144	0.183	0.196	0.162	0.155	0.182	0.194	0.323	0.307	0.117	0.150	0.187	0.152	0.155	0.177	0.202	0.157
Lu	0.024	0.022	0.026	0.024	0.028	0.030	0.025	0.023	0.026	0.028	0.048	0.045	0.021	0.024	0.029	0.023	0.023	0.028	0.033	0.024

Table 2

	JNdi-1	MS-177
$I^{145}Nd$ (V)	0.7 - 1.5	0.64
$\mu^{142}Nd$	0.0 ± 5.6	-10.9 ± 5.7
$\mu^{143}Nd$	0.0 ± 7.4	640 ± 4.9
$\mu^{145}Nd$	0.0 ± 4.4	5.7 ± 4.1
$\mu^{148}Nd$	0.0 ± 8.2	9.9 ± 7.4
$\mu^{150}Nd$	0.0 ± 10.9	11.5 ± 11.5
^{142}Ce ppm	0.4	1.2
^{144}Sm ppm	0.4	0.3
n	6	1
$^{147}Sm/^{144}Nd$		0.1896
$\mu^{142}Nd$ A		-1.4
$\mu^{142}Nd$ B		-1.1
$\varepsilon^{143}Nd$, 4.568 Ga		0.06

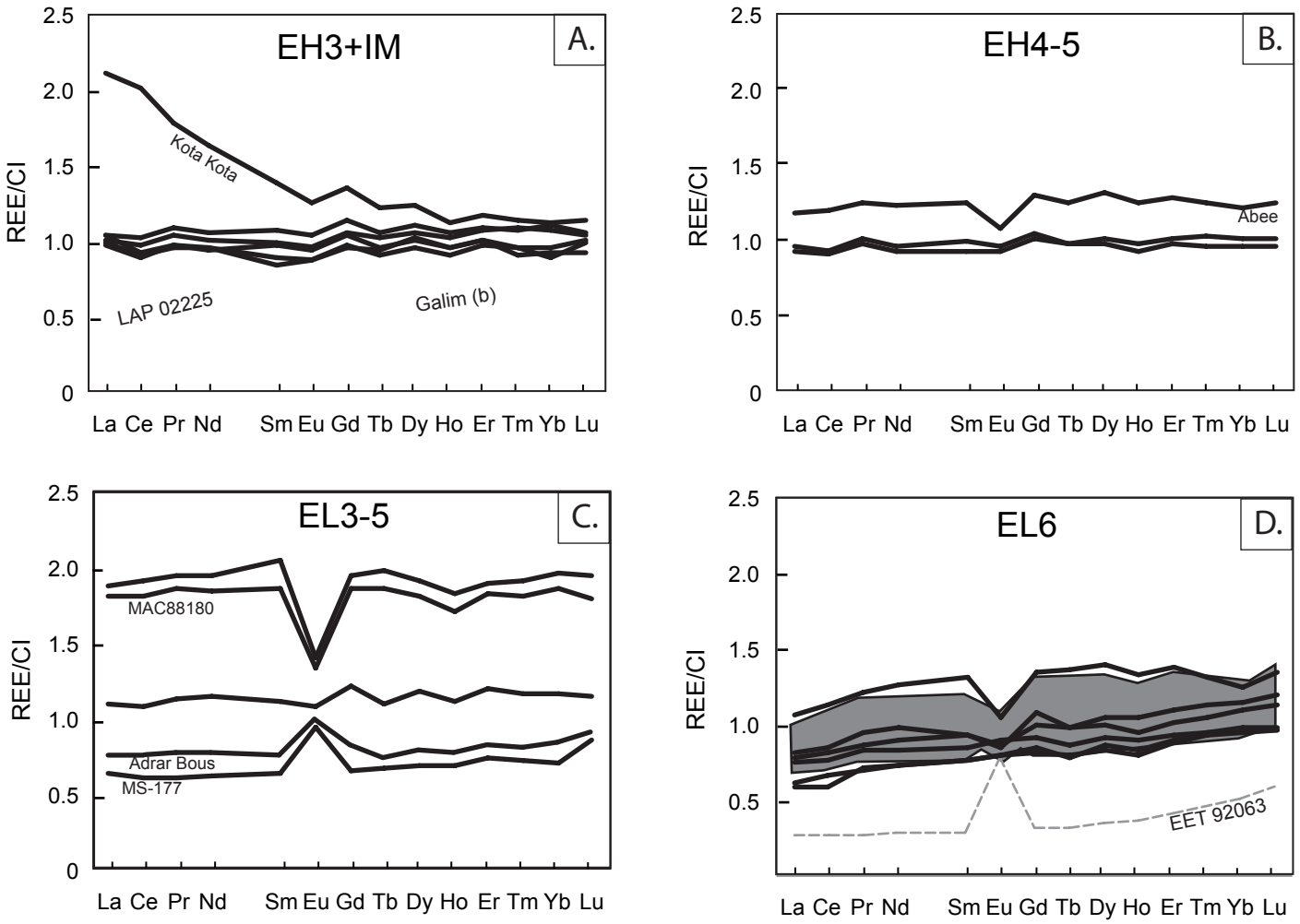
EH3+IM
A.
Kota Kota
LAP 02225
Galim (b)
EH4-5
B.
Abee
EL3-5
C.
MAC88180
Adrar Bous
MS-177
EL6
D.
EET 92063
REE/CI
2.5
2.0
1.5
1.0
0.5
0
La Ce Pr Nd Sm Eu Gd Tb Dy Ho Er Tm Yb Lu

Figure 1

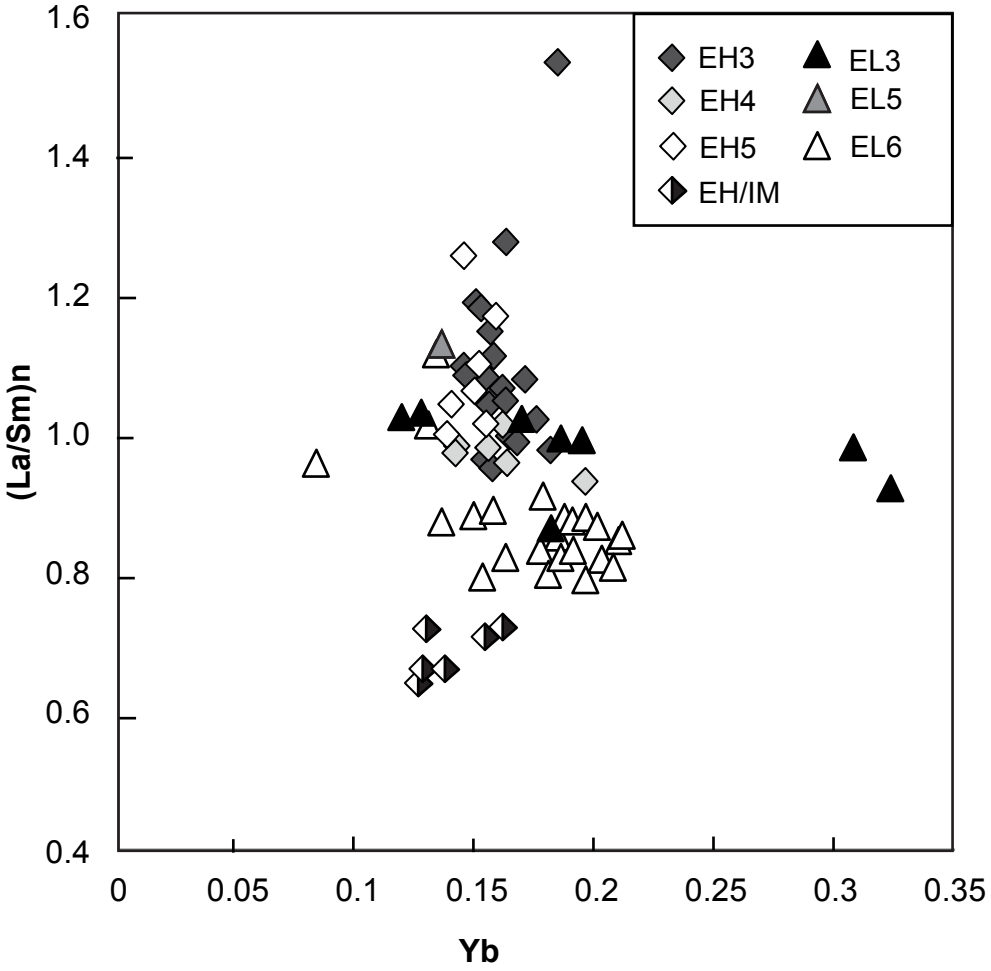
EH3
EH4
EH5
EH/IM
EL3
EL5
EL6
(La/Sm)n
Yb
1.6
1.4
1.2
1.0
0.8
0.6
0.4
0
0.05
0.1
0.15
0.2
0.25
0.3
0.35

Figure 2.

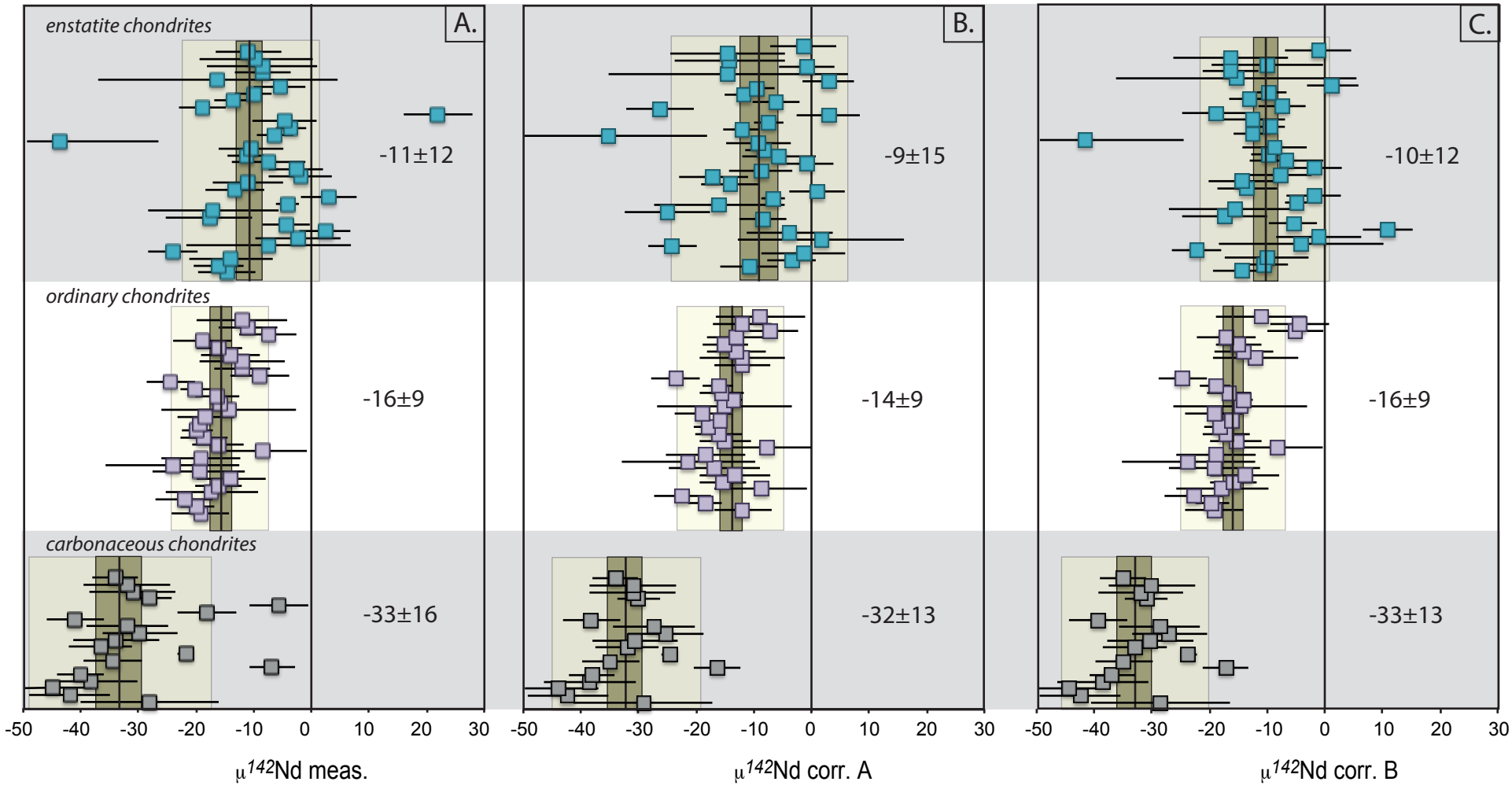
A.
B.
C.
enstatite chondrites
ordinary chondrites
carbonaceous chondrites
-11±12
-16±9
-33±16
-9±15
-14±9
-32±13
-10±12
-16±9
-33±13
-50 -40 -30 -20 -10 0 10 20 30
μ142Nd meas.
μ142Nd corr. A
μ142Nd corr. B

Figure 3.

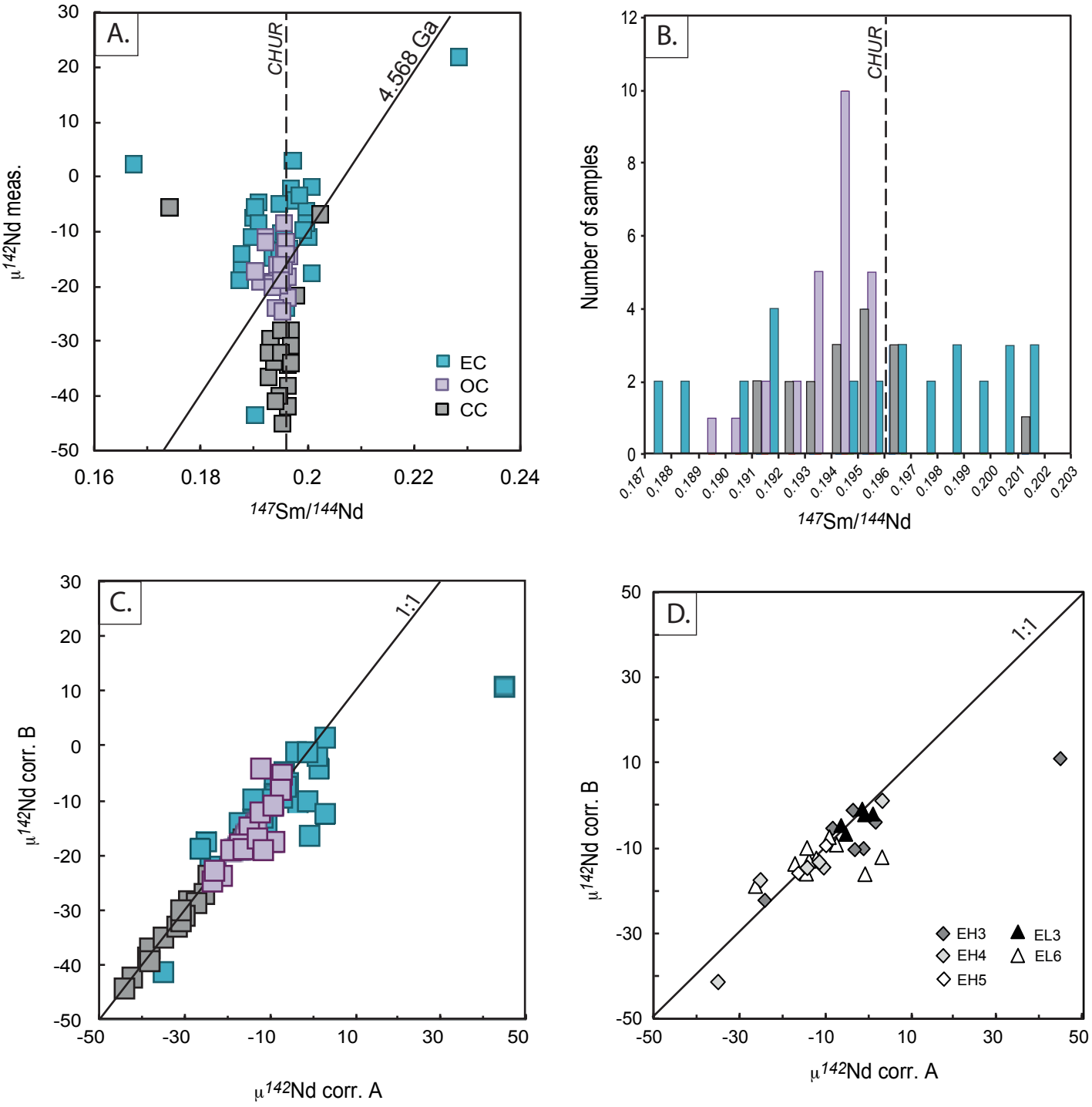
A.
CHUR
4.568 Ga
EC
OC
CC
μ142Nd meas.
147Sm/144Nd
B.
CHUR
Number of samples
147Sm/144Nd
C.
1:1
μ142Nd corr. B
μ142Nd corr. A
D.
1:1
EH3
EH4
EH5
EL3
EL6
μ142Nd corr. B
μ142Nd corr. A

Figure 4

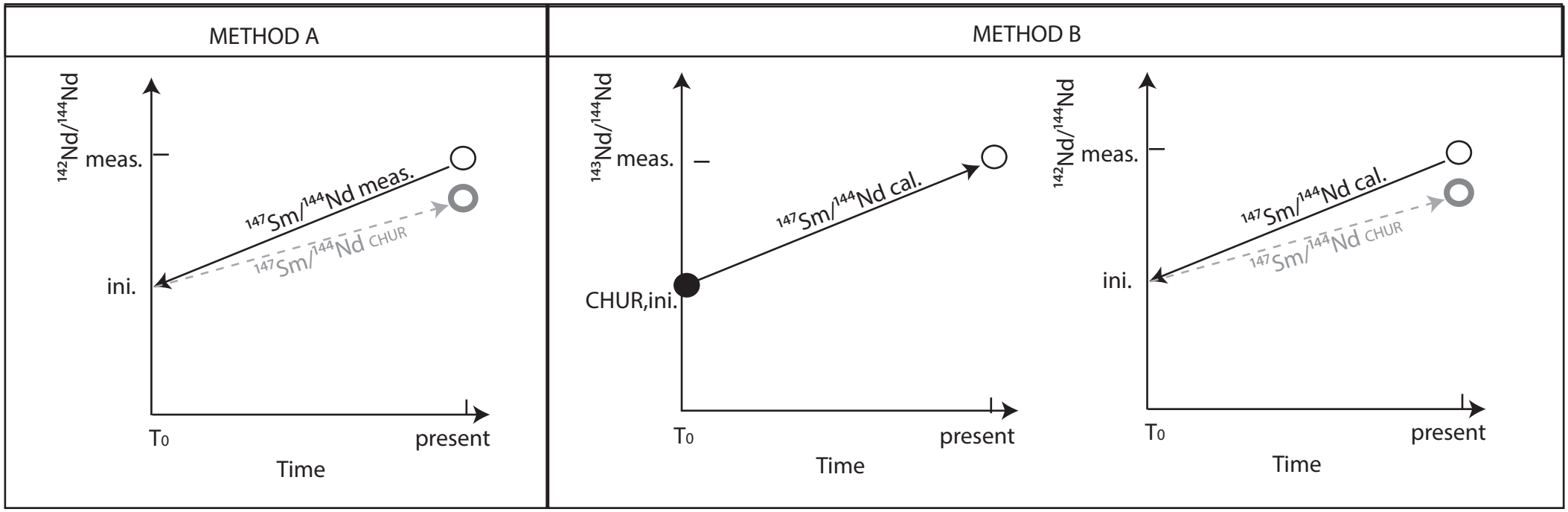
METHOD A
METHOD B
$^{142}Nd/^{144}Nd$
meas.
ini.
$^{147}Sm/^{144}Nd$ meas.
$^{147}Sm/^{144}Nd$ CHUR
T0
present
Time
$^{143}Nd/^{144}Nd$
meas.
CHUR,ini.
$^{147}Sm/^{144}Nd$ cal.
T0
present
Time
$^{142}Nd/^{144}Nd$
meas.
ini.
$^{147}Sm/^{144}Nd$ cal.
$^{147}Sm/^{144}Nd$ CHUR
T0
present
Time

Figure 5

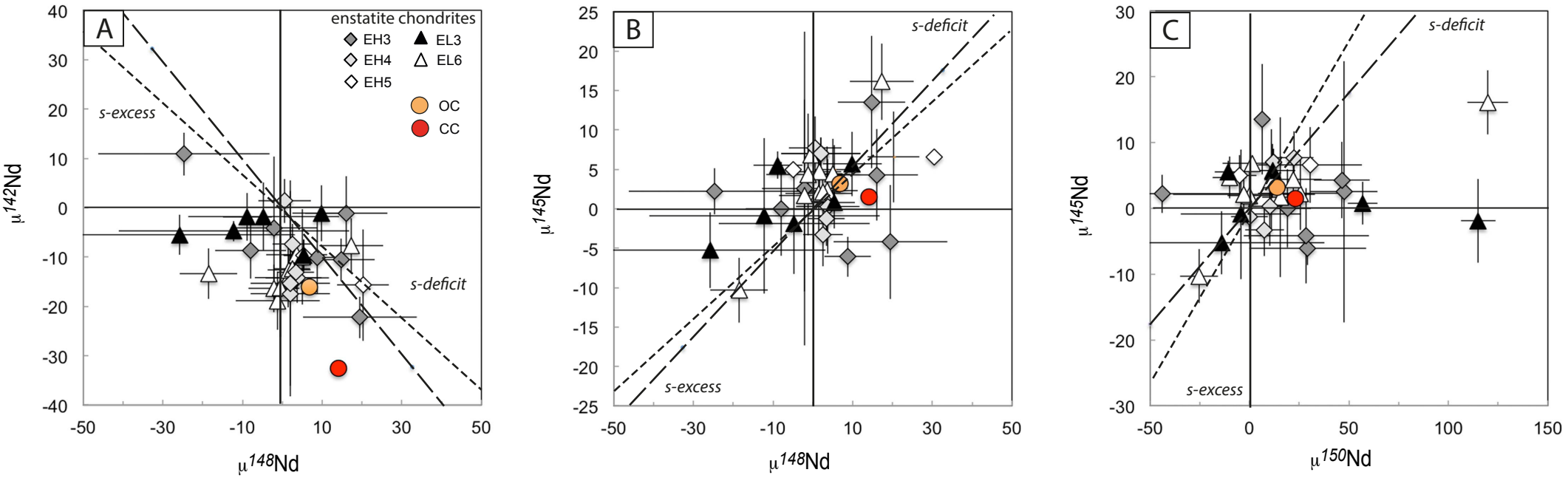
A
enstatite chondrites
EH3
EH4
EH5
EL3
EL6
OC
CC
s-excess
s-deficit
μ142Nd
μ148Nd
B
s-deficit
s-excess
μ145Nd
μ148Nd
C
s-deficit
s-excess
μ145Nd
μ150Nd

Figure 6.

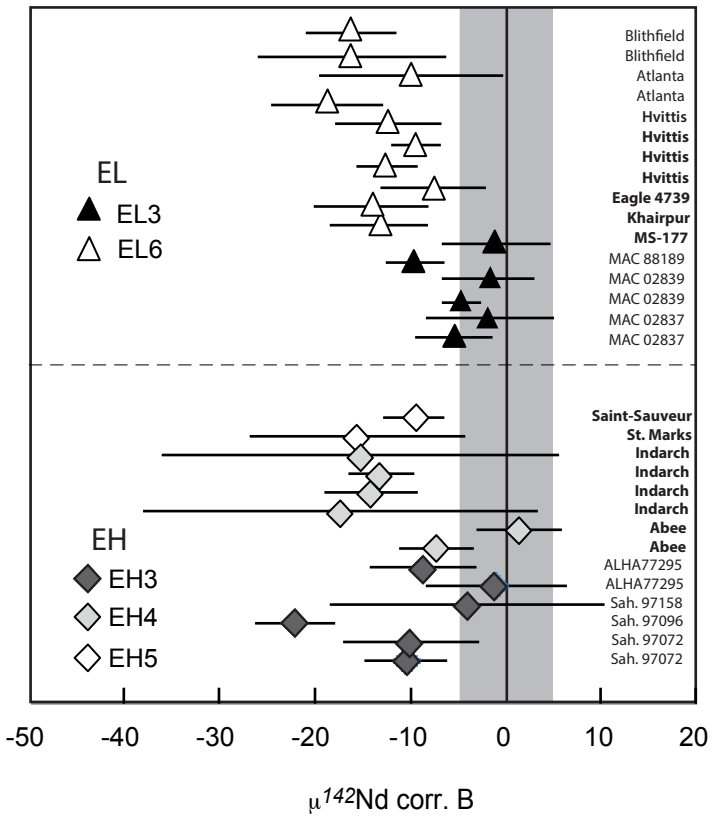
EL
EL3
EL6
EH
EH3
EH4
EH5
Blithfield
Blithfield
Atlanta
Atlanta
Hvittis
Hvittis
Hvittis
Hvittis
Eagle 4739
Khairpur
MS-177
MAC 88189
MAC 02839
MAC 02839
MAC 02837
MAC 02837
Saint-Sauveur
St. Marks
Indarch
Indarch
Indarch
Indarch
Abee
Abee
ALHA77295
ALHA77295
Sah. 97158
Sah. 97096
Sah. 97072
Sah. 97072
-50
-40
-30
-20
-10
0
10
20
μ142Nd corr. B

Figure 7

Table S1.
Compilation from:
Boyet and Carlson 2005 **Rankenburg et al., 2006**
Carlson et al., 2007 **Gannoun et al., 2011**
Bouvier and Boyet 2016 **Burkhardt et al., 2016**
Fukai and Yokoyama 2017

Name	Type	$\mu^{142}Nd$	$\mu^{143}Nd$	$\mu^{145}Nd$	$\mu^{148}Nd$	$\mu^{150}Nd$	2S* $\mu^{142}Nd$	2S* $\mu^{143}Nd$	2S* $\mu^{145}Nd$	2S* $\mu^{148}Nd$	2S* $\mu^{150}Nd$	$\mu^{142}Nd$ corr A	u142 corr B	$^{147}Sm/^{144}Nd$	Reference
Carbonaceous chondrites															
Orgueil	CI-Fall	-28.0	1000.7	-25.3	4.1	1.3	12.0	*5.0*	13.0	20.0	28.0	-29.2	-28.5	0.1968	Carlson et al., Science 2007
Cold Bokkveld	CM2-Fall	-41.9	1001.7	2.6	25.7	42.3	7.0	*5.0*	7.0	12.0	17.0	-42.2	-42.4	0.1962	Carlson et al., Science 2007
Mighei	CM2-Fall	-45.0	960.5	8.0	50.5	88.8	7.0	*5.0*	7.0	13.0	18.0	-44.0	-44.4	0.1953	Carlson et al., Science 2007
Murray	CM2-Fall	-38.2	997.2	4.9	28.6	29.2	8.0	*5.0*	8.0	15.0	19.0	-38.5	-38.5	0.1962	Carlson et al., Science 2007
Allende	CV3-Fall	-40.0	858.8	13.2	30.2	26.2	4.0	*5.0*	5.0	8.0	11.0	-38.1	-36.9	0.1947	Carlson et al., Science 2007
Grosnaja	CV3-Fall	-6.8	1396.1	-12.1	7.9	18.2	4.0	*5.0*	4.0	6.0	10.0	-16.3	-17.2	0.2024	Carlson et al., Science 2007
Mokoia	CV3-Fall	-34.4	1001.3	1.7	21.9	39.8	5.0	*5.0*	5.0	8.0	11.0	-34.9	-34.9	0.1963	Carlson et al., Science 2007
Allende	CV3-Fall	-21.8	1101.2	-1.8	8.7	14.1	1.5	6.7	15.4	19.9	32.5	-24.6	-23.6	0.1979	Gannoun et al., PNAS 2011
Allende	CV3-Fall	-36.6	889.3	4.0	7.3	4.8	5.5	4.5	3.8	7.2	10.3	-32.0	-32.9	0.1930	Boyet and Carlson 2005
Allende	CV3-Fall	-33.9	891.8	4.4	-2.3	-20.7	7.5	6.3	5.4	9.6	13.3	-30.6	-30.3	0.1938	Boyet and Carlson 2005
Allende Bomb	CV3-Fall	-29.7	924.4	0.3	-6.3	-27.9	6.5	5.4	4.5	8.2	10.9	-25.3	-27.0	0.1929	Boyet and Carlson 2005
Allende	CV3-Fall	-32.0	904.2	1.6	1.0	-12.5	7.1	5.6	5.4	9.8	13.2	-27.4	-28.7		Boyet and Carlson 2005
Allende	CV3-Fall	-41.0	966.6	3.0	6.0	118.0	5.0	0.0				-38.2	-39.3	0.1941	Rankenburg et al., 2006
Allende (2)	CV3-Fall	-30.0	1076.2	2.0	9.0	8.0	5.0	1.4	9.0	4.0	24.0	-30.0	-31.0		Burkhardt et al. (2016)
Allende (3)	CV3-Fall	-30.0	1088.4	5.0	4.0	-6.0	6.0	3.1	6.0	7.0	24.0	-31.0	-32.0		Burkhardt et al. (2016)
Allende (4)	CV3-Fall	-33.0	1000.6	8.0	16.0	11.0	8.0	2.6	13.0	15.0	31.0	-31.0	-33.0		Burkhardt et al. (2016)
Dho 1432	CR2-Found	-28.0		16.0	18.0	26.0	3.8		15.0	5.4	9.5	-26.0	-30.0	0.195	Fukai and Yokoyama 2017
Murchison	CM2-Fall	-31.0		2.1	23.0	24.0	7.4		16.0	13.0	24.0	-32.0	-31.0	0.197	Fukai and Yokoyama 2017
Allende	CV3-Fall	-32.0		-1.1	19.0	27.0	7.5		16.0	16.0	26.0	-30.0	-31.0	0.195	Fukai and Yokoyama 2017
DaG 190	CO3-Found	-34.0		19.0	22.0	27.0	4.0		27.0	4.6	7.4	-35.0	-34.0	0.197	Fukai and Yokoyama 2017
Tagish Lake	C2-ungrouped-Fall	*-18.0*		*-4.9*	*3.2*	*8.7*	*5.1*		*16.0*	*5.9*	*11.0*			*0.148*	*Fukai and Yokoyama 2017*
NWA 2090	CO3-Fall	*-5.6*		*-6.7*	*0.8*	*4.3*	*5.1*		*48.0*	*5.9*	*11.0*			*0.174*	*Fukai and Yokoyama 2017*
Ordinary chondrites															
Gladstone	H6-Find	-19.2	982.6	2.9	3.3	9.3	5.0		6.0	11.0	14.0	-11.9	-19.2	0.1911	Carlson et al., Science 2007
Homestead	L5-Fall	-19.8	974.4	-2.0	8.7	12.7	3.0		3.0	6.0	8.0	-18.5	-19.6	0.1951	Carlson et al., Science 2007
Ucera	H5-Fall	-22.0	1013.0	-2.6	21.1	122.6	5.0		6.0	10.0	13.0	-22.4	-22.7	0.1963	Carlson et al., Science 2007
Peace River	L6-Fall	-17.3	1004.4	22.1	0.4	26.2	8.0		9.0	14.0	19.0	-8.8	-17.8	0.1903	Carlson et al., Science 2007
Sharps	H3-Fall	-16.2	1024.9	8.5	1.6	-13.3	4.1	3.3	3.1	5.0	7.7	-15.4	-15.9	0.1959	Boyet and Carlson 2005
Sharps	H3-Fall	-13.9	1033.7	7.2	-2.4	-13.2	6.1	5.2	4.5	8.1	11.5	-13.2	-13.9	0.1951	Boyet and Carlson 2005
Richardton (Bomb)	H5-Fall	-19.5	1020.9	3.6	8.7	-29.7	8.0	6.5	6.1	11.3	14.8	-16.9	-19.2	0.1942	Boyet and Carlson 2005
Richardton	H5-Fall	-24.0	1020.9	3.1	22.9	-19.4	11.6	9.3	9.2	16.7	21.6	-21.4	-23.7	0.1942	Boyet and Carlson 2005
Dhajala	H3-Fall	-19.2	1021.5	3.9	-3.8	-0.5	6.9	5.6	4.8	8.2	12.1	-18.3	-18.9	0.1954	Boyet and Carlson 2005
Bruderheim	L6-Fall	-8.5	1020.2	2.8	-16.3	-27.3	7.7	6.3	5.8	10.6	13.9	-7.7	-8.1	0.1955	Boyet and Carlson 2005
Allegan	H5-Fall	-16.1	1005.9	5.2	11.3	25.1	4.5	3.9	4.9	6.2	11.8	-15.0	-15.4	0.1952	Burkhardt et al., 2016
Forest City	H5-Fall	-18.6	974.9	5.2	3.6	7.3	4.1	9.4	7.3	14.6	37.1	-16.2	-17.0	0.1944	Burkhardt et al., 2016
Queens Mercy	H6-Fall	-19.8	971.3	1.9	6.1	16.0	2.7	2.5	2.8	15.8	46.1	-17.7	-18.2	0.1946	Burkhardt et al., 2016
Bruderheim	L6-Fall	-19.4	904.6	2.4	0.9	11.8	0.9	2.2	0.0	15.2	49.6	-15.7	-16.1	0.1935	Burkhardt et al., 2016
Chelyabinsk	LL5-Fall	-18.3	1068.6	2.4	2.6	7.6	5.0	7.7	0.8	9.4	1.8	-18.8	-19.2	0.1963	Burkhardt et al., 2016
Dhurmsala	LL6-Fall	-14.3	1048.8	0.2	9.2	21.9	11.6	7.5	8.5	4.7	25.7	-15.1	-14.6	0.1965	Burkhardt et al., 2016
Farmington	L5-Fall	-15.9	945.2	9.6	9.8	23.8	1.5	4.4	8.1	6.4	4.2	-13.5	-14.0	0.1944	Burkhardt et al., 2016
Ste. Marguerite	H4-Fall	-16.3	1031.8	9.6	11.1	21.2	3.9	0.5	4.2	2.7	13.4	-15.6	-16.6	0.1955	Burkhardt et al., 2016
Pultusk	H5-Fall	-20.1	975.2	12.9	10.7	18.2	2.6	7.5	7.3	5.3	19.1	-16.2	-19.0	0.1934	Burkhardt et al., 2016
Ste. Marguerite (2)	H4-Fall	-24.4	1029.2	10.1	6.4	17.5	4.2	14.9	15.0	17.6	0.6	-23.5	-24.7	0.1954	Burkhardt et al., 2016
Kesen	H4-Fall	-12.0		-4.4	15.0	27.0	4.9		14.0	4.9	12.0		-12.0		Fukai and Yokoyama 2017
Forest City	H5-Fall	-12.0		17.0	11.0	17.0	7.4		27.0	7.6	19.0	-12.0	-12.0	0.196	Fukai and Yokoyama 2017
Saratov	L4-Fall	-14.0		6.8	13.0	20.0	5.1		16.0	5.9	11.0	-14.0	-13.0	0.196	Fukai and Yokoyama 2017
Etter	L5-Found	-16.0		-12.0	8.9	19.0	4.0		27.0	4.6	7.4	-15.0	-15.0	0.195	Fukai and Yokoyama 2017
Modoc (1905)	L6-Fall	-19.0		-6.1	8.1	6.0	5.1		16.0	5.9	11.0	-17.0	-13.0	0.195	Fukai and Yokoyama 2017
Hamlet	LL4-Fall	-7.5		2.4	10.0	35.0	4.9		15.0	5.1	12.0	-5.1	-7.2		Fukai and Yokoyama 2017
Tuxtuac	LL5-Fall	-11.0		-7.3	6.4	13.0	5.1		16.0	5.9	11.0	-4.3	-12.0	0.192	Fukai and Yokoyama 2017
Saint-Séverin	LL6-Fall	-12.0		-5.7	10.0	23.0	7.8		14.0	12.0	12.0	-11.0	-8.9	0.192	Fukai and Yokoyama 2017
Adrian	H4-Found	*-8.9*		*-7.5*	*-1.0*	*-1.7*	*5.1*		*16.0*	*5.9*	*11.0*			*0.1370*	*Fukai and Yokoyama 2017*
Enstatite chondrites															
Indarch	EH4-Fall	-14.6	969.7	0.3	3.7	10.2	5.0		6.0	8.0	11.0	-10.8	-14.3	0.1934	Carlson et al., Science 2007
SAHARA 97072	EH3-Found	-16.1	808.7	13.5	14.7	6.4	4.3	3.5	8.4	8.4	3.1	-3.4	-10.6	0.1875	Gannoun et al., PNAS 2011
SAHARA 97072	EH3-Found	-14.0	872.6	-6.1	8.8	29.2	7.3	2.2	2.5	5.8	29.4	-1.3	-10.1	0.1875	Gannoun et al., PNAS 2011
SAHARA 97096	EH3-Found	-24.0	957.3	-4.2	19.5	28.5	4.3	6.3	7.2	14.3	31.5	-24.1	-22.2	0.1961	Gannoun et al., PNAS 2011
SAHARA 97158	EH3-Found	-7.4	895.1	2.5	-2.0	47.5	14.4	17.7	19.9	10.7	17.0	1.7	-4.1	0.1899	Gannoun et al., PNAS 2011
ALHA77295	EH3-Found	-2.3	982.0	4.3	16.1	46.4	7.4	6.3	5.8	10.4	14.1	-3.7	-1.1	0.1970	Gannoun et al., PNAS 2011
MAC 02837	EH3-Found	-4.4	1071.7	-5.3	-25.8	-14.1	4.1	0.7	4.8	29.0	51.8	-8.4	-5.5	0.1987	Gannoun et al., PNAS 2011
Indarch	EH4-Fall	-17.7	1014.9	2.0	0.7	4.3	7.4	12.5	6.4	0.0	36.6	-25.0	-17.4	0.2009	Gannoun et al., PNAS 2011
St. Mark's	EH5-Fall	-17.0	974.3	6.6	20.3	30.4	11.3	9.9	5.8	6.5	26.2	-16.0	-15.7	0.1953	Gannoun et al., PNAS 2011
MAC 02839	EL3-Found	-4.2	1049.3	-0.9	-12.2	-4.3	2.1	4.8	9.9	29.0	30.4	-6.6	-4.8	0.1976	Gannoun et al., PNAS 2011
MAC 88180	EL3-Found	3.1	1224.7	5.5	-8.8	-10.8	4.8	4.1	1.7	6.2	6.9	1.0	-1.9	0.1974	Gannoun et al., PNAS 2011
Khairpur	EL6-Fall	-13.2	1034.1	-10.3	-18.5	-25.4	5.1	4.4	4.1	7.2	9.5	-14.0	-13.4	0.1965	Gannoun et al., PNAS 2011
Eagle	EL6-Fall	-10.9	1156.1	1.9	1.5	0.1	6.0	5.0	4.7	8.3	11.2	-17.0	-14.2	0.2001	Gannoun et al., PNAS 2011
Hvittis	EL6-Fall	-1.8	1261.7	16.1	17.3	119.8	5.5	4.9	4.9	8.1	10.2	-8.8	-7.7	0.2007	Gannoun et al., PNAS 2011
MAC 02837	EL3-Found	-5.0	999.4	-1.9	-4.7	115.0	6.8	2.7	6.4	19.0	8.6	-0.8	-1.8	0.1948	Bouvier and Boyet 2016
MAC 02339	EL3-Found	-11.4	960.5	0.8	5.4	56.9	3.2	3.9	3.3	5.2	7.6	-8.2	-9.6	0.1939	Bouvier and Boyet 2016
ALHA 77295	EH3-Found	-10.4	963.7	0.0	-7.9	19.0	5.6	6.5	5.9	9.0	11.8	-9.1	-8.7	0.1951	Bouvier and Boyet 2016
Hvittis (1)	EL6-Fall	-6.3	1285.4	4.7	1.7	-10.0	3.2	2.7	3.2	5.4	8.5	-12.1	-12.6	0.1999	Burkhardt et al., 2016
Hvittis (2)	EL6-Fall	-3.5	1262.7	2.3	3.6	25.6	2.6	3.1	5.6	7.7	21.4	-7.4	-9.5	0.1986	Burkhardt et al., 2016
Atlanta	EL6-Fall	-4.6	1332.1	2.1	2.5	-2.9	5.5	7.3	2.4	4.6	35.7	2.9	-12.4	0.1909	Burkhardt et al., 2016
Abee (1)	EH4-Fall	-18.9	562.5	-3.3	2.6	7.6	4.0	3.1	4.0	5.0	9.7	-6.1	-7.4	0.1874	Burkhardt et al., 2016
Indarch	EH4-Fall	-13.5	1006.2	-1.3	3.4	0.0	3.4	2.9	3.4	4.6	9.3	-11.8	-13.1	0.1948	Burkhardt et al., 2016
Saint-Sauveur	EH5-Fall	-10.0	1023.7	5.0	5.5	-4.9	3.2	2.5	3.2	5.0	8.5	-9.4	-9.7	0.1956	Burkhardt et al., 2016
Abee (2)	EH4-Fall	-5.5	745.3	7.7	0.6	22.4	4.5	3.1	4.0	6.6	9.7	3.0	1.4	0.1903	Burkhardt et al., 2016
Indarch (2)	EH4-Fall	-16.3	981.2	7.0	2.0	12.0	20.8	6.6	2.0	10.0	3.0	-14.5	-15.3	0.1948	Burkhardt et al., 2016
Atlanta (2)	EL6-Found	-8.4	1334.5	1.7	-2.1	15.4	4.8	8.6	12.2	6.4	9.0	-0.8	-16.3	0.1909	Burkhardt et al., 2016
Blithfield (2)	EL6-Found	-8.5	1075.3	4.4	5.1	22.0	9.7	0.0	4.5	2.3	14.4	-14.2	-10.0	0.1998	Burkhardt et al., 2016
Hvittis (3)	EL6-Fall	-9.6	1284.6	6.8	-0.5	1.5	9.9	0.6	0.0	0.6	15.0	-14.5	-16.3	0.1993	Burkhardt et al., 2016
MS-177	EL3-Fall	-10.9	640.0	5.7	9.9	11.5	5.7	4.9	4.1	7.4	11.5	-1.4	-1.1	0.1896	This study
Abee	EH4-fall	-43.6	950.5	-17.0	-31.4	-32.9	17.1	15.3	17.4	28.4	32.7	-35.1	-41.5	0.1903	Boyet and Carlson 2005
Kota-Kota	EH3-Found	2.4	689.4	2.2	-24.7	-44.0	4.4	4.1	2.9	21.5	40.9	44.7	10.9	0.1675	Gannoun et al., PNAS 2011
Blithfield (1)	EL6-Found	22.0	2651.4	4.3	-1.1	10.9	5.9	1.9	7.7	10.5	3.6	-26.2	-18.8	0.2285	Burkhardt et al., 2016

*Uncertainties on individual samples are internal errors (2SE) or external errors (2SD) when several measurements have been performed.

Carbonaceous Chondrites															
ALL															
n = 12	mean	-30.5		2.0	13.6	20.5						-31.8	-32.3	0.1920	
	weighted mean	-31.4		1.4	15.1	16.1						-23.4	-23.7		
	2SD	20.1		18.5	26.6	65.3						13.0	12.5	0.0246	
	95% conf.	4.4		4.1	5.9	14.5						3.0	2.9	0.0061	
	2SE	4.3		3.9	5.7	13.9						2.9	2.8		
	n	22		22	22	22						20	20	18	
Carbonaceous Chondrites															
-Tagish Lake and NWA2090															
n = 10	mean	-32.4		2.8	14.7	21.9						-31.8	-32.3	0.1959	
	weighted mean	-33.1		4.1	15.9	16.7						-32.3	-32.8		
	2SD	16.3		18.7	26.9	68.0						13.0	12.5	0.0046	
	95% conf.	3.8		4.1	5.9	14.5						3.0	2.9	0.0012	
	2SE	3.7		4.2	6.0	15.2						2.9	2.8	0.0011	
	n	20		20	20	20						20	20	16	
Ordinary Chondrites															
ALL															
n = 25	mean	-16.4		3.2	6.8	13.7						-14.8	-16.0	0.1924	
	weighted mean	-16.2		2.1	6.5	13.1						-13.7	-15.4		
	2SD	8.8		15.1	15.2	53.4						9.3	8.7	0.0224	
	95% conf.	1.7		2.9	2.9	10.1						1.8	1.7	0.0044	
	2SE	1.6		2.8	2.8	9.9						1.8	1.7	0.0043	
	n	29		29	29	29						27	28	27	
Ordinary Chondrites															
-Adrian															
n = 24	mean	-16.7		3.6	7.1	14.2						-14.8	-16.0	0.1946	
	weighted mean	-16.4		2.7	6.6	13.5						-14.2	-15.9		
	2SD	8.5		14.8	15.2	54.0						9.3	8.7	0.0033	
	95% conf.	1.6		2.9	2.9	10.5						1.8	1.7	0.0007	
	2SE	1.6		2.8	2.9	10.2						1.8	1.7	0.0006	
	n	28		28	28	28						27	28	26	
Enstatite Chondrites															
ALL															
n = 19	mean	-9.6		1.8	0.2	15.4						-8.0	-10.5	0.1950	
	weighted mean	-12.1		0.5	-5.6	8.0						-10.4	-12.7		
	2SD	20.7		12.6	24.9	69.3						26.4	17.7	0.0084	
	95% conf.	3.7		2.3	4.5	12.5						4.8	3.2	0.0016	
	2SE	3.7		2.2	4.4	12.2						4.7	3.1	0.0016	
	n	32		32	32	32						32	32	29	
Enstatite Chondrites															
-Abee B&C 2005, Kota Kota, Blithfield (1)															
n = 17	mean	-9.9		2.3	2.1	19.3						-8.3	-9.8	0.1950	
	weighted mean	-10.6		2.2	-1.2	15.4						-8.9	-10.3		
	2SD	12.1		11.1	21.0	66.4						14.8	11.5	0.0084	
	95% conf.	2.3		2.1	4.0	12.6						2.8	2.2	0.0016	
	2SE	2.2		2.1	3.9	12.3						2.8	2.1	0.0016	
	n	29		29	29	29						29	29	29	
Enstatite Chondrites EL3															
n=4															
	mean	-5.7		1.8	-2.1	33.7						-3.2	-3.8	0.1947	
	weighted mean	-1.3		-0.3	-7.2	4.6						-0.7	-0.8		
	2SD	11.8		12.5	23.7	75.0						7.9	7.0	0.0065	
	95% conf.	7.3		4.1	5.9	14.5						4.9	4.4	0.0040	
	2SE	5.3		5.6	10.6	33.5						3.6	3.1	0.0029	
	n	5.0		5.0	5.0	5.0						5.0	5.0	5.0	
Enstatite Chondrites EL6															
n=5															
	mean	-7		3	1	16						-10	-12	0.1974	
	weighted mean	-8.0		2.8	1.3	13.5						-10.5	-12.7		
	2SD	7.4		13.6	18.5	84.0						13.5	6.0	0.0078	
	95% conf.	2.8		5.2	7.1	32.3						5.2	2.3	0.0030	
	2SE	2.5		4.5	6.2	28.0						4.5	2.0	0.0026	
	n	9.0		9.0	9.0	9.0						9.0	9.0	9.0000	

Table S2.
Nd compositions of MS-177 and terrestrial samples

	Nd (ng)	I145 (V)	$^{142}Nd/^{144}Nd$	2SE	$^{143}Nd/^{144}Nd$	2SE	$^{145}Nd/^{144}Nd$	2SE	$^{148}Nd/^{144}Nd$	2SE	$^{150}Nd/^{144}Nd$	2SE	$^{142}Ce/^{142}Nd$ (ppm)	$^{144}Sm/^{144}Nd$ (ppm)	N
JNdi-1_F1R1	500	0.97	1.141852	0.000006	0.512110	0.000002	0.348403	0.000001	0.241576	0.000002	0.236445	0.000002	0.7	0.4	540
JNdi-1_F1R2	500	0.97	1.141850	0.000005	0.512112	0.000002	0.348403	0.000001	0.241578	0.000001	0.236445	0.000002	0.2	0.3	900
JNdi-1_F2R1	500	1.28	1.141847	0.000004	0.512110	0.000001	0.348403	0.000001	0.241579	0.000001	0.236446	0.000001	0.3	0.4	900
JNdi-1_F3R1	500	1.68	1.141853	0.000003	0.512111	0.000001	0.348403	0.000001	0.241579	0.000001	0.236448	0.000001	0.3	0.5	900
JNdi-1_F4R1	250	0.70	1.141844	0.000006	0.512108	0.000002	0.348402	0.000001	0.241579	0.000002	0.236448	0.000002	0.4	0.3	900
JNdi-1_F5R1	250	1.48	1.141851	0.000004	0.512114	0.000002	0.348404	0.000001	0.241579	0.000001	0.236448	0.000002	0.3	0.5	720
JNdi-1_F6R1	250	0.97	1.141852	0.000004	0.512112	0.000002	0.348403	0.000001	0.241579	0.000001	0.236446	0.000002	0.34	0.42	900
Mean JNdi-1			1.141850		0.512111		0.348403		0.241578		0.236446		0.4	0.4	
2s			0.000006		0.000004		0.000002		0.000002		0.000003				
2s (ppm)			5.6		7.4		4.4		8.2		10.9				
n			7		7		7		7		7				
MS177_F9R1	300	0.64	1.141838	0.000007	0.512439	0.000002	0.348405	0.000001	0.241581	0.000002	0.236448	0.000002	1.2	0.3	640